Pterosin B,ingredient in Pteridium aquilinum,regulates hepatic gluconeogenesis via SIK3-dependent and independent mechanisms.

論文博士

学位授与年月: **2017.3**

関西大学審査学位論文

Pterosin B, ingredient in *Pteridium aquilinum*, regulates hepatic gluconeogenesis via SIK3-dependent and independent mechanisms.

2016

Yumi Itoh

博士論文要旨

近年、食生活の欧米化により糖尿病患者数は増加の一途を辿っており、その対策が急務となっている。糖尿病は心疾患や脳血管障害に繋がる恐れがあり、食習慣の改善で解決されない場合は、薬剤による血糖値のコントロールが必要となる。糖尿病に対する薬剤の選択肢は幅広いが、根本治療は達成できておらず、新たな作用機序に基づく血糖値制御因子の探索とその制御法の開発が望まれる。

肝臓における糖新生は、空腹時に糖を合成することで血糖値を高める役割があり、血糖値上昇要因の一つである。一方で、糖尿病患者では糖新生が恒常的に亢進しており、糖新生を阻害する薬剤は血糖値を低下させる。糖新生はグルカゴン-cyclic AMP（cAMP）シグナルにより制御されており、様々な酵素とその遺伝子の発現に関与する転写調節因子が関与する。それに関連する転写調節因子の代表として、cAMP-response element-binding protein（CREB）やその共役因子(CREB regulated transcription coactivator 2, CRTC2)が挙げられる。

塩誘導性キナーゼ（Salt Inducible Kinase, SIK）は CREB-CRTC2 を抑制するため、SIK の活性化剤が糖尿病に有効であると予想される。SIK には３つのアイソフォームがあり、これまでに、マウス肝臓の SIK1 タンパク質を欠損させると、血糖値が上昇することが明らかにされている。さらに SIK2 も糖代謝において抑制的に機能していることが報告されている。しかしながら、SIK3 の糖代謝における役割は未だ明らかにされていない。本研究では、SIK3 シグナル阻害剤を同定し、その阻害剤の SIK3 依存的・非依存的な肝糖新生制御メカニズムの解明を行った。

第１章：SIK3 遺伝子破壊マウスにおける SIK3 の糖新生における役割

SIK3 遺伝子破壊マウス（SIK3-KO マウス）を用いて、SIK3 の糖代謝への影響を検討した。SIK3-KO マウスは痩せ型であり、極度な低血糖を示すことが明らかとなった。しかしながら、SIK3-KO マウスの肝臓における糖新生関連遺伝子の発現は有意に上昇していた。SIK3-KO マウスは痩せ型を示しているため、体内のエネルギー不足（空腹状態）により二次的に糖新生が亢進している可能性が示唆された。そこで、二次的影響を除外した条件下で SIK3 の糖新生における役割を確認するため、SIK3 による CRTC2 の遺伝子発現の抑制を阻害する化合物（SIK3 シグナル阻害剤）の探索・同定を行った。SIK3 シグナル阻害剤は、遺伝子の活性を発光強度として観測することが出来るレポーターアッセイシステムを利用して探索・同定した。その結果、ワラビ成分である Pterosin B が SIK3 シグナル阻害活性を示すことを判明し、その阻害によって糖新生関連酵素の遺伝子発現を上昇させることを示した。すなわち、肝臓では SIK3 シグナルを阻害すると血糖値上昇に繋がると示唆された。

第２章：SIK3 シグナル阻害剤 Pterosin B を用いた SIK3 依存的な肝糖新生制御メカニズムの解明

第１章において同定した SIK3 シグナル阻害剤 Pterosin B を用いて、SIK3 依存的な糖新生制御メカニズムの解明を行った。Pterosin B が SIK3 の直接阻害剤では無かったことから、Pterosin B の作用部位としての SIK3 の上流因子を探索した。その結果、Pterosin B はグリコーゲンの分解を刺激するキナーゼ Phosphorylase kinase catalytic subunit gamma2 (PHKG2)の SIK3 への結合性を上昇させ、SIK3 抑制ドメインのリン酸化を亢進させることで SIK3 シグナルを阻害することが示唆された。以上の結果から、Pterosin B は PHKG2 を介して SIK3 を阻害し、肝臓における糖新生を亢進させることが示され、SIK3 が肝糖新生において重要な役割を果たすことが示唆された。

第３章：Pterosin B の SIK3 非依存的な肝糖新生制御メカニズムの解明

第２章において、Pterosin B は SIK3 を介して肝糖新生を亢進させることが示された。しかしながら、Pterosin B の類似体である Pterosin A は血糖値低下作用を有することが報告されている。そこで、生体レベルにおける Pterosin B の血糖値への影響を検討するため、糖尿病モデルマウスに Pterosin B を混餌した飼料を与えたところ、コントロール飼料群に比べて血糖値が低下しており、SIK3 阻害による糖新生亢進とは矛盾する結果となった。そこで、Pterosin B の糖新生における新たな役割の解明を行うことにした。単離したマウス初代肝細胞を用いて、糖新生を亢進させるホルスコリン（Forskolin, Fsk）存在下におけるグルコース産生実験を行った結果、Fsk により活性化した糖新生は、Pterosin B により抑制されることが示された。さらに、マウス肝臓由来の培養細胞を用いて、Fsk 依存的な糖新生関連遺伝子の発現亢進時における Pterosin B の影響を検討したところ、Pterosin B は糖新生の最終ステップ酵素 glcose-6-phosphatase（G6Pc）の発現を抑制することが示された。これは、*G6pc* のプロモーターにおける Retinoic acid receptor-related orphan receptor alpha-steroid receptor coactivator 2 (RORα-SRC2) 複合体の結合阻害に起因していることがレポーターアッセイにより明らかとなった。さらに、Pterosin B はミトコンドリア呼吸鎖の Coenzyme Q の酸化還元サイクルに異常をきたし、細胞内の ATP レベルを低下させることを示唆した。ミトコンドリア呼吸鎖複合体 III の阻害剤 Antimycin A も Pterosin B と同様に、RORα-SRC2 複合体を阻害して *G6pc* の遺伝子発現を抑制することが明らかとなり、RORα-SRC2 複合体はミトコンドリア呼吸鎖の Coenzyme Q の酸化還元サイクル異常を感知して *G6pc* の発現を調節している可能性が示唆された。以上の結果から、Pterosin B は G6pc への RORα-SRC2 複合体の結合を阻害して、糖新生の最終ステップ G6Pc の発現を抑制することで血糖値を低下させると結論した。

以上

TABLE OF CONTENTS

Section Page

Introduction ・・・・・・・3

CHAPTER 1

The role of SIK3 on hepatic gluconeogenesis

1-1. Introduction ・・・・・・・5

1-2. Results ・・・・・・・7

1-3. Discussion ・・・・・・・23

1-4. Reference ・・・・・・・24

CHAPTER 2

Pterosin B regulates hepatic gluconeogenesis via a SIK3-dependent mechanism.

2-1. Introduction ・・・・・・・28

2-2. Results ・・・・・・・28

2-3. Discussion ・・・・・・・40

2-4. Reference ・・・・・・・42

CHAPTER 3

Pterosin B regulates hepatic gluconeogenesis via a SIK3-independent mechanism.

3-1. Introduction ・・・・・・・44

3-2. Results ・・・・・・・45

3-3. Discussion ・・・・・・・58

3-4. Reference ・・・・・・・60

Summary ・・・・・・・62

Experimental Section ・・・・・・・64

Abbreviation ・・・・・・・77

List of Publications ・・・・・・・79

Conference presentations ・・・・・・・82

Acknowledgement ・・・・・・・84

Introduction

The number of patients suffering from lifestyle-related diseases, diabetes, hyperlipidemia, and hypertension have been increasing by the western lifestyles. Once lifestyle-related diseases are developed, a continuous medication is required.

In the case of diabetes, the number of patients tends to increase from 470 million in 1980 to over 2000 million in 2014. Seriously diabetic patients need insulin supplementation and some develop renal insufficiency followed by hemodialysis, resulting in a reduced quality of life.

Diabetes is classified as type I and type II. Type I diabetes is due to a lack of insulin, therefore, patients in type I diabetes require insulin injection. On the other hand, type II diabetes is caused by a decrease of insulin secretion or insulin resistance. Patients in type II diabetes are prescribed medications to control blood glucose level.

Blood glucose levels are maintained by a balance between glucose uptake/storage/utilization and glucose production, gluconeogenesis. Gluconeogenic program in hepatocytes is important for providing glucose to peripheral tissues under a fasting state. However, gluconeogenesis is up-regulated not only under fasting but also under feeding state in patients with diabetes, resulting in hyperglycemia.

Hepatic gluconeogenesis is regulated by two rate-limiting enzymes, phosphoenolpyruvate carboxykinase (PEPCK), and glucose-6-phosphatase catalytic subunit (G6PC). Gene expressions of these enzymes are up-regulated in patients with diabetes.

5′-AMP-activated protein kinase (AMPK) is a serine/threonine kinase that function as

intracellular energy sensor. AMPK is activated under conditions that increase AMP levels such as glucose deprivation and excess exercise. Once activated, AMPK phosphorylates a number of downstream targets, resulting in the improvement of not only glucose metabolism but also lipid metabolism. Therefore, AMPK is considered to be a key therapeutic target for the treatment of metabolic diseases such as type II diabetes and obesity. Metformin used for the treatment of type II diabetes lowers blood glucose levels by regulation of hepatic gluconeogenesis via the activation of AMPK in an insulin-dependent manner, therefore hypoglycemia is rarely caused. However, it has been reported that not only metformin but also other therapeutic agents for diabetes have side effects. For example, metformin is contraindication to kidney diseases, because it is metabolized in the kidneys. Therefore, it is needed that new regulators for glucose metabolism have to develop to treat diabetes.

CHAPTER 1

The role of SIK3 on hepatic gluconeogenesis

1-1. Introduction

Salt-inducible kinase (SIK) is a member of AMPK-related kinase family, and the SIK-subfamily is composed of three isoforms (1). SIK1 was isolated from the adrenals of rats fed with a high Na+ or K+ diet (2). SIK2 was identified by its sequence similarity (3). SIK3 was characterized by another group in a wide range analysis (4). Although multiple SIK-substrates have been identified based on information from the SIK phosphorylation motifs, Lx(R/K)(S/T)xpSxxxL (pS:phospho-Ser) (5), only two types of substrates, CRTC (a coactivator for the cAMP response element (CRE)-binding protein (CREB)) and class IIa histone deacetylase (HDAC) (6), have been confirmed by independent research groups. Phosphorylation of these two substrates by SIKs results in a loss of their transcriptional regulatory activities by inducing nuclear export (5,7). The other important aspect of SIK is as a feedback regulator in cAMP-activated protein kinase (PKA) signaling (8). When PKA activates CREB by phosphorylation, it also counters SIK actions by phosphorylating SIK's C-terminal regulatory domain, which in turn promotes the dephosphorylation rate of CRTC, enhances nuclear accumulation of this coactivator, and increases CREB-dependent gene expression (5,7,9). Conversely, when PKA activity wanes, the reactivated SIK terminates CREB activity by inactivating CRTC (5,9). This is also the case for class IIa-HDAC (6). PKA-dependent inactivation SIK facilitates the activation of class IIa-HDAC. Because class IIa-HDAC is the major

suppressor of myocyte enhancer factor 2 (MEF2) (10), the MEF2-dependent transcription is suppressed by PKA and reactivated by SIK(6). The first physiological relevance of SIKs *in vivo* was found in the mouse liver as a suppression of gluconeogeneic programs (11). CREB is one of the key transcription factors that upregulate gluconeogenic gene expression (12) by binding to their gene promoters, such as *phosphoenolpyruvate carboxykinase* (*Pepck*), *glucose-6-phosphatase catalytic subunit* (*G6pc*), and *peroxisome proliferator-activated receptor gamma coactivator 1α* (*Pgc1a*: formal gene name was *Ppargc1a*). The knockdown of SIK1 protein in the mouse liver by RNAi-adenovirus vectors results in an increase in blood glucose levels, which is accompanied by the dephospho-form of CRTC2 and enhanced levels of gluconenogenic gene expression (11). However, the effects of SIK1-knockout (KO) on glucose metabolism have not been elucidated (13). SIK2 also may play an important role in glucose metabolism (3,14-17).

Previous reports have shown that SIKs are related to glucose and lipid metabolism. However, it has not been elucidated whether SIK3 has a role on glucose metabolism or not. In this chapter, the involvement of SIK3 in glucose metabolism is demonstrated by using SIK3-KO mice and their hepatocytes.

1-2. Results

Characterization of SIK3-KO mice

The body weight of SIK3-KO mice was obviously less than that of the wild type mice. (Fig.1-1A). 1-year-old mice showed that the lean phenotype of SIK3-KO mice was attributed to the liver and adipose tissues, especially mesenteric and perirenal fat (Fig.1-1B). Small but substantial amounts of gonadal and subcutaneous fat and brown adipose tissue were observed in SIK3-KOmice. The low levels of liver TG in *Sik3*$^{-/-}$ mice might have prevented the development of fatty liver (Fig.1-1C), while total cholesterol levels were low in the serum of SIK3-KO mice.

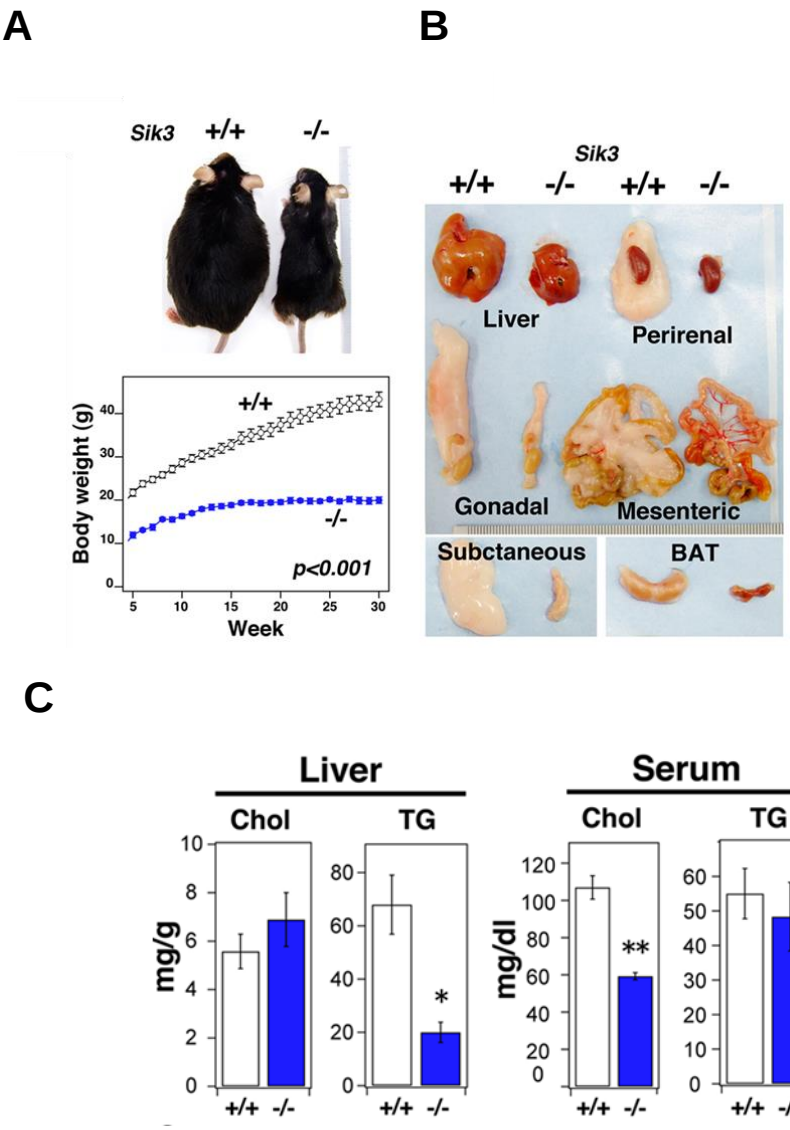

Fig.1-1. SIK3-KO mice are lean and hypolipidemic.

(A) The body weight of male mice (n = 6) was monitored. All data points show p,0.001. (B) One-year-old male mice (n = 5) were sacrificed (scale: 1 mm). (C) Cholesterol (Chol) and triglycerides (TG) in the liver and serum were measured (n = 5).

Next, blood glucose levels were examined. In the fed condition, the SIK3-KO mice had slightly lower blood glucose levels than the wild-type mice, and the levels quickly decreased after fasting (Fig.1-2A). After a 4-h fast, the SIK3-KO mice had significantly lower serum insulin and leptin levels than the wild-type mice (Fig. 1-2B), while no obvious differences were observed in free FA or ketone body (β-hydroxybutyrate) levels.

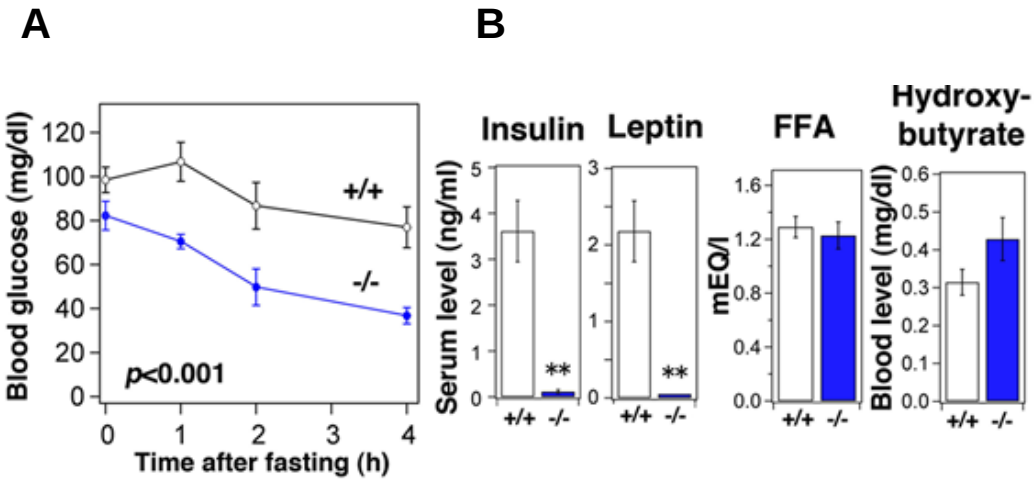

Fig.1-2. SIK3-KO mice are hypoglycemic.
(A) Mice (n = 5) were fasted and their blood glucose levels were monitored at the indicated time points. All data points show p,0.001. (B) After 4-h fasting, the serum levels of insulin, leptin, free fatty acid (FFA), and ß-hydroxybutyrate were measured.

SIK3-KO mice exhibited enhanced glucose tolerance (GTT) (Fig.1-3A). When SIK3-KO mice were treated with insulin (ITT), their blood glucose levels decreased like those of the wild-type mice (Fig.1-3B). Once the SIK3-KO mice were supplied exogenously with an energy source, such as lactate (lactate tolerance test), they were able to produce glucose efficiently (Fig.1-3C), suggesting that the hypoglycemia of SIK3-KO mice may be due to a lack of energy storage followed by an enhanced insulin response.

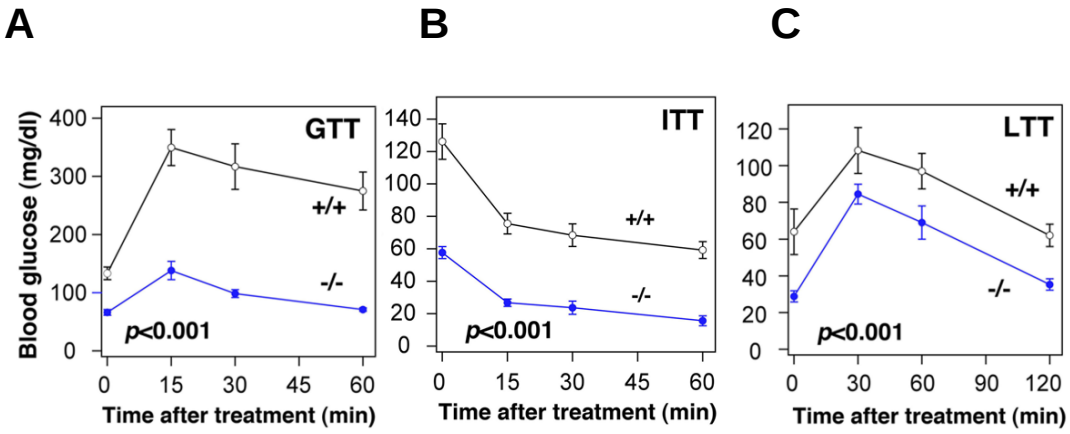

Fig.1-3. SIK3-KO mice are lean, hypolipidemic, and hypoglycemic.

(A) After 4-h fasting, glucose (1.5 g/kg) was intraperitoneally injected (GTT, glucose tolerance test) and blood glucose levels were monitored (n = 5). (B)

(C) After 24-h fasting, lactate (1.5 g/kg) was injected intraperitoneally (LTT, lactate tolerance test; n = 5).

The gene expression profile of the liver (Fig.1-4A) indicated that the pathway from glycolysis to FA synthesis was down-regulated in *Sik3*$^{-/-}$ mice, while the glyconeogenic pathway was up-regulated. *Sik3*$^{-/-}$ mice expressed high levels of *Fgf21* mRNA, suggesting an adaptive response to starvation; however, its promoting pathway, *i.e.*, the peroxisome proliferator-activated receptor alpha (PPARα) pathway, was down-regulated. Lack of FA storage and the uncoupling of FGF21 from the PPARα pathway in *Sik3*$^{-/-}$ mice may result in the failure to induce β-oxidation followed by ketogenesis (18).

Next, the state of signaling molecules was examined. The high level of PGC-1α protein in the liver of *Sik3*$^{-/-}$ mice was accompanied by the dephosphorylation of CRTC2 (Fig.1-4B) despite there being no significant difference in the status of CREB. Interestingly, the level of another CRTC2 kinase, AMPK (11), and of its activated phosphorylated form (pThr172) were also high in the livers of *Sik3*$^{-/-}$ mice. Immunohistochemical analyses revealed the enhanced accumulation of CRTC2 in the nuclei of *Sik3*$^{-/-}$ mice hepatocytes (Fig.1-4C). In addition, HDAC5, another SIK/AMPK substrate (19,20), also accumulated in the nuclei of liver cells in *Sik3*$^{-/-}$ mice, suggesting that AMPK is unable to compensate for the deficiency of SIK3 in hepatocytes.

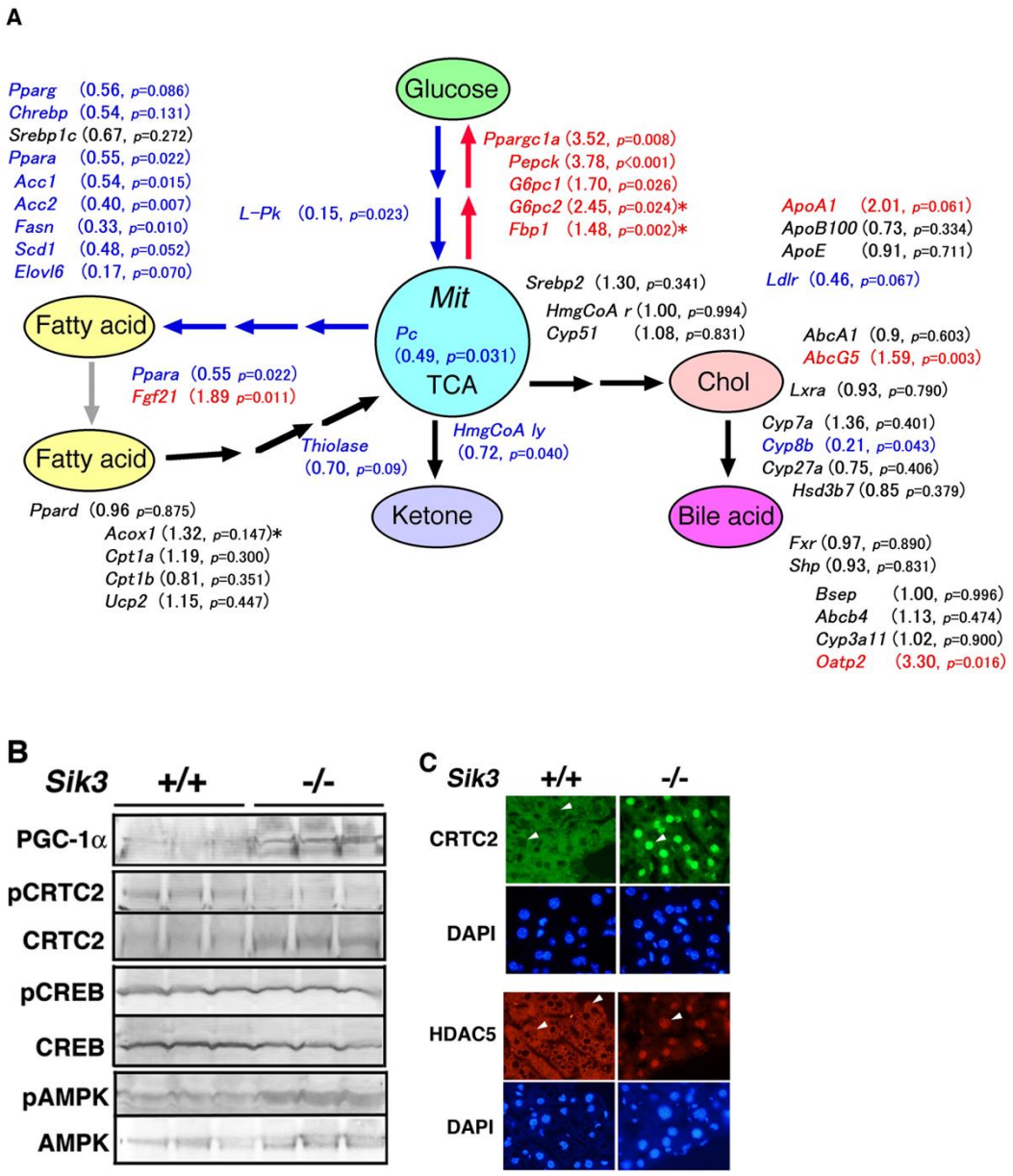

Fig.1-4. Gene expression profile in the liver.

(A) One-year-old male mice (n = 5) were fasted for 4 h, and the liver mRNA levels were measured using quantitative polymerase chain reaction (qPCR). Red and blue indicate the up- and down-regulated genes in Sik32/2 mice, respectively. +, fold increase; -, fold decrease. The threshold is set at p=0.1. The values marked with an asterisk (*) were obtained using PCR-array kits (n = 3). The abbreviations for the genes and the PCR primers used are listed in Table S2. Mit, mitochondria; TCA, tricarboxylic acid cycle. (B) Intracellular signaling molecules and their activation status in the liver were examined by western blot analysis. (C) Immunohistochemical analysis of SIK3 substrates (CRTC2 and HDAC5) in the liver.

Gluconeogenic program is constitutively up-regulated in SIK3-KO Mice.

In cultured cell systems, SIK1-3 regulates energy metabolism by apparently sharing the same transcriptional modulators, CRTCs (21), and ClassIIa-HDACs (22). *In vivo*, however, only SIK3-KO mice had dramatic phenotypes for energy metabolism. To confirm the indispensability of SIK3 in glucose metabolism *in vivo*, all SIKs KO mice, with the same genetic background (C57BL/6J), were subjected to a glucose challenge after 4 h of starvation (Fig. 1-5A). Although the blood glucose levels in both the WT and SIK3-KO mice were significantly elevated in response to the glucose treatment, the maximum level was significantly lower in the SIK3-KO than WT mice. However, no significant difference in glucose clearance between the SIK1-KO or SIK2-KO mice and their WT mice was observed. Next, the gluconeogenic potency in these mice was tested by performing a lactate (a source of gluconeogenesis) challenge under a fed condition in which the gluconeogenic programs had not been run in the WT liver due to insulin actions. The blood glucose levels in the SIK3-KO mice were quickly increased to the levels of the WT mice after lactate treatment, while there was no significant response in the glucose level to lactate in WT, SIK1-KO, or SIK2-KO mice
(Fig. 1-5B), suggesting a constitutively activated gluconeogenic ability in the SIK3-KO mice.

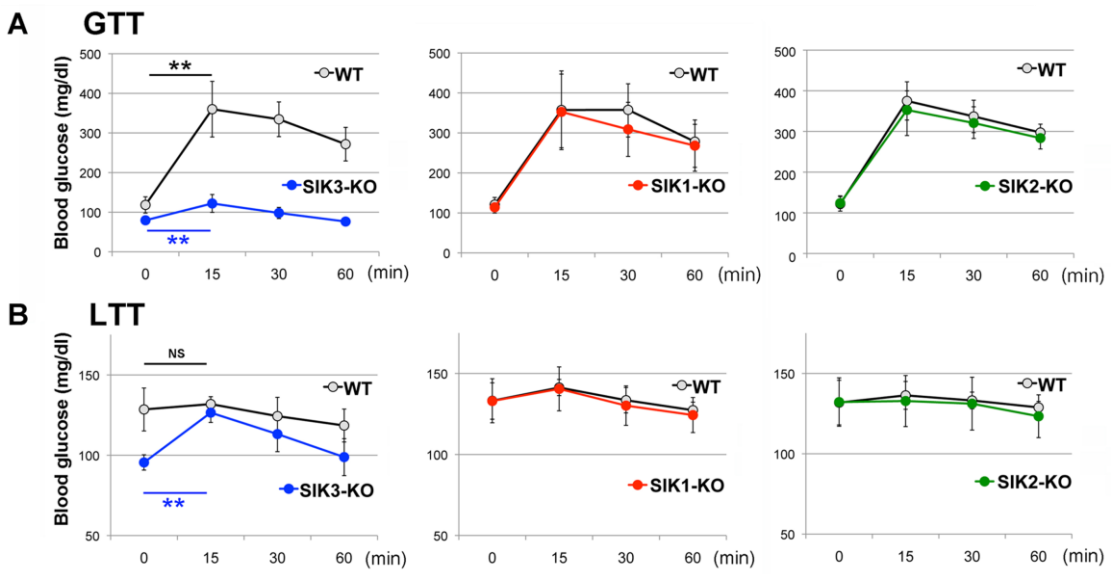

Fig.1-5. Glucose metabolism in SIK1-3 KO mice.

(A) WT and SIK1-3 KO mice (8-week-old females n = 6) were starved for 4 h (4 h after lights were on) and subjected to a glucose tolerance test (1.5 g/kg); the blood glucose level was measured. Means and SD were indicated. **, $p < 0.01$ compare to 0 time. (B) A lactate tolerance test (1.5 g/kg) was performed under the fed condition (just after the light was turned on).

Gluconenogenic programs in SIK3-KO hepatocytes

Although the gluconeogenic gene expression has been upregulated in SIK3-KO mouse liver not in SIK1-KO and SIK2-KO mouse liver, the systemic effects, *e.g.*, hypoglycemia, made it difficult to discuss the cell autonomous actions in the SIK3-KO mouse liver. To eliminate systemic effects, primary hepatocytes from SIK3-KO mice were prepared.

Gene expression analyses (Fig.1-6A, genes related to gluconenogenesis: *Pgc1a, Pepck, and G6pc*) suggested that SIK3-KO hepatocytes possessed a high gluconeogenic potency even in unstimulated cells with almost fully enhanced gluconeogenic gene expression levels. Briefly, starvation (glucose-/glutamate-free) did not alter gluconeogenic gene expression levels in both WT and SIK3-KO mice hepatocytes. The stimulation of WT hepatocytes with Fsk upregulated the levels of gluconenogenic gene expression up to (*Pgc1a and Pepck*) or beyond (*G6pc*) those increased levels in the SIK3-KO hepatocytes. Western blot analyses (Fig.1-6B) detected a constitutively-dephosphorylated CRTC2 in the SIK3-KO hepatocytes.

Curiously, Fsk-induced phosphorylation of CREB was not observed in the SIK3-KO hepatocytes. AMPK had already been phosphorylated in unstimulated SIK3-KO hepatocytes, suggesting an energy-depleted environment in SIK3-KO hepatocytes; however, the starved condition might not the major factors for the enhanced gluconeogenic programs in SIK3-KO mice hepatocytes.

A

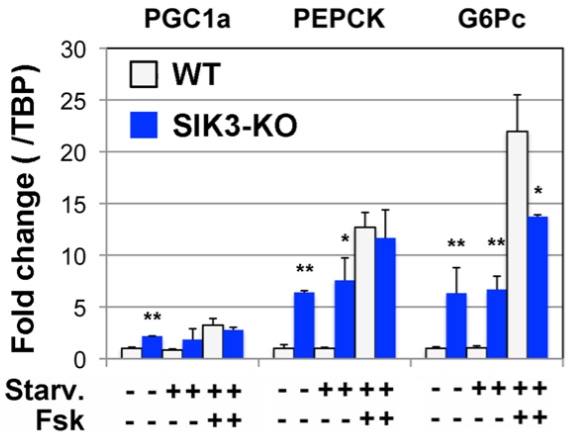

B

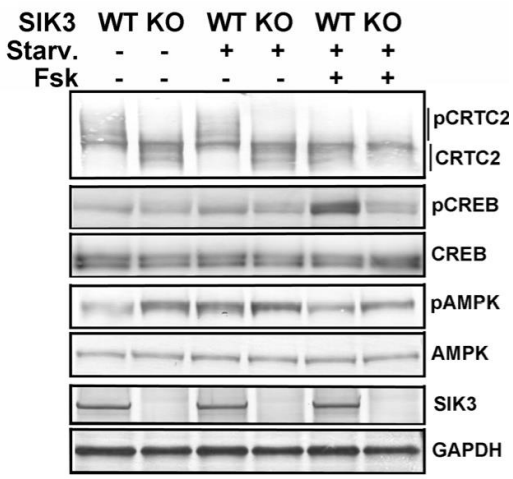

Fig.1-6. Enhanced gluconenogenic programs in SIK3-KO hepatocytes.

(A) The hepatocytes were pre-incubated with a low serum (1%) medium for 12 h and incubated in a serum-free medium, a starvation medium alone, or supplemented with 20 μM Fsk for 3 h. Total RNA was extracted for qPCR. (n = 3). The same treatment was used for western blot analyses (B).

To confirm the glucose production from SIK3-KO hepatocytes, glucose production was induced by lactate, Fsk and dexamethasone. As shown in Fig.1-7, the SIK3-KO hepatocytes produced glucose more quickly than the WT hepatocytes (at 2 h post-Fsk treatment), despite a lower maximum glucose production (at 8 h).

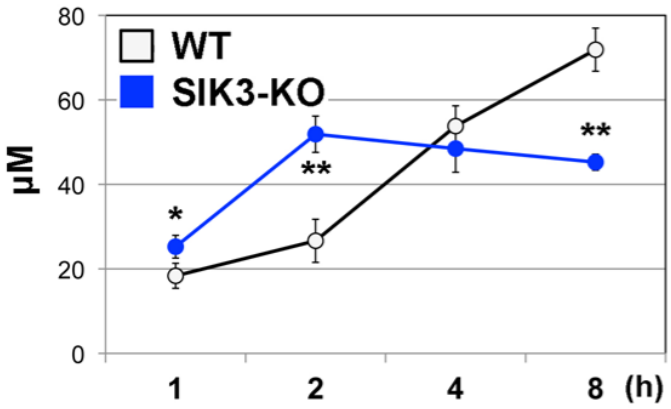

Fig.1-7. Enhanced glucose production in SIK3-KO hepatocytes.

Hepatocytes were prepared from 8-week-old female mice (n=3 or 4) and cultured in a low serum (1%) medium for 12 h. Then cells were pretreated with a starvation medium (serum- and glucose-/glutamate-free) for 1 h. Glucose production was induced by 10 mM lactate, 20 μM Fsk, and 0.1 μM dexamethasone. Means and SD were indicated. *, $p < 0.05$; **, $p < 0.01$.

Identification of SIK3 signaling inhibitor

To precisely characterize the SIK3 actions in defined culture systems, the mouse hepatoma AML-12 cells was used. Despite a successful knockdown of SIK1 and SIK2 protein in AML-12 cells, SIK3 protein was hardly eliminated. Moreover, an *in vitro* screening for SIK3 inhibitors from our chemical library (~2,500 compounds) resulted in only an identification of non-specific inhibitors, such as the flavonoid fisetin (23). To identify an inhibitor of the SIK3-specific signal, reporter-based screening using transcription regulators (class IIa-HDAC and CRTC2) that were suppressed by SIKs was used. Fig.1-6A indicates the principles of the reporter system. Because SIK3 inhibited the suppressive action of class IIa-HDAC on the transcription factor MEF2, the firefly luciferase (fLuc) activity under the regulation of the GAL4 fusion MEF2 is upregulated by SIK3 and downregulated by the SIK3 inhibitory compounds, such as the non-specific kinase inhibitor staurosprine (STS) (21) (Fig.1-8B). CRTC2 is also inhibited by SIK3; thus, the *Renilla* by LEXA-fusion CRTC2 was suppressed by SIK3, and STS upregulated the LEXA-rLuc activity. The combination of these two reporters in the same cells produced approximately 25 times the S/N ratio, when SIK3 was inhibited by STS. Using these reporters and HEK293 cells, pterosin B, an ingredient in *Pteridium aquilinum*, was identified as a candidate for SIK3 signaling inhibition (Fig.1-8C). The action of pterosin B on MEF2 and CRTC2 were also confirmed in separately assayed fLuc reporter systems in the AML-12 cells (Fig.1-8D). The structural-activity relationship assay suggested that only pterosin S failed to inhibit SIK3 signaling (Fig.1-8E). Synthetic pterosin B (racemic) also inhibited SIK3 signaling, indicating that pterosin B, not non-pterosin contaminants, inhibited SIK3 signaling.

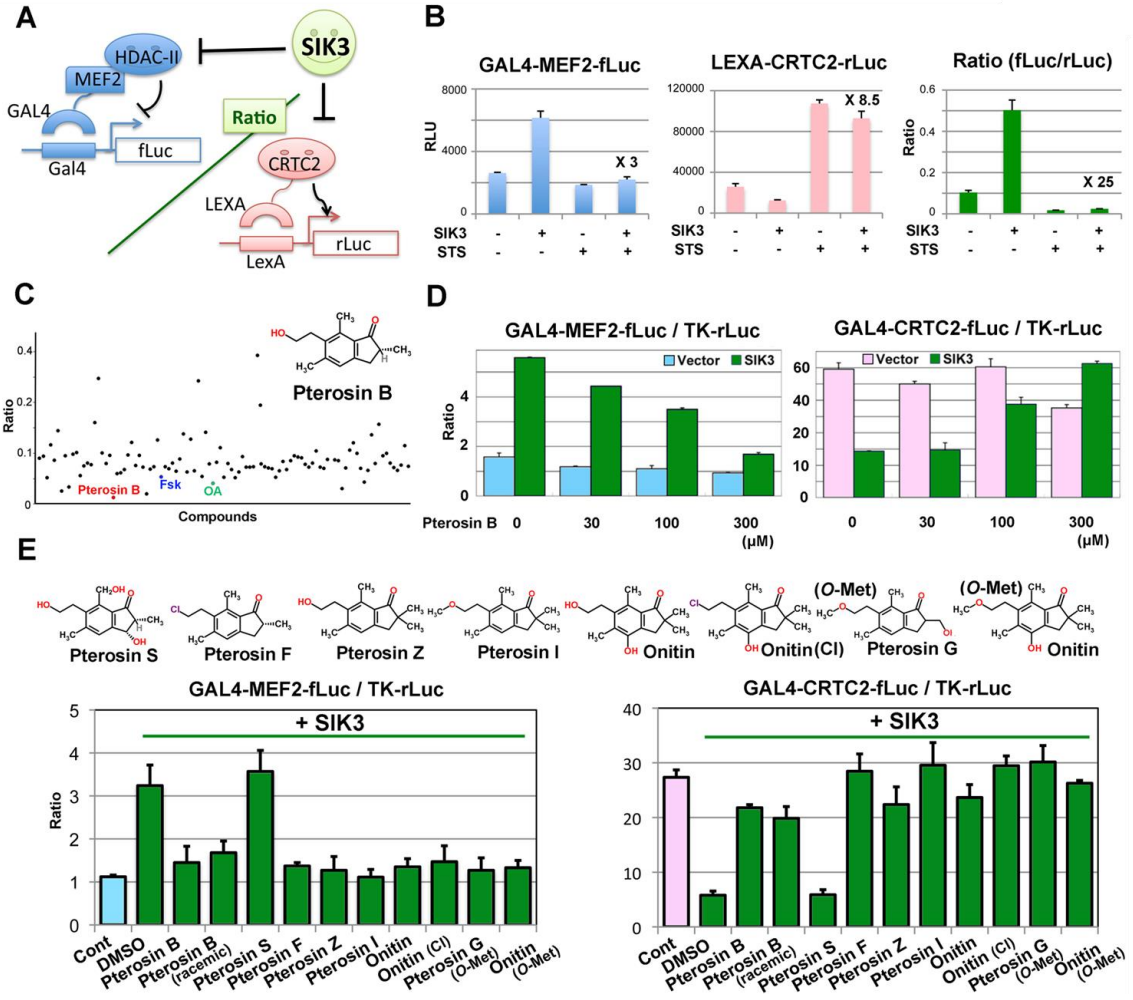

Fig.1-8. Pterosin B inhibits SIK3 signaling.

(A) A principle of reporter-based chemical screening. (B) A model experiment of reporter assays using the non-specific kinase inhibitor staurosporine (STS, 10 nM). The fold difference in un-normalized luciferase activities between SIK3-overexpression alone and SIK3 + STS was indicated (n = 3). (C) The result of a representative plate containing pterosin B was indicated. Fsk (20 μM) and Okadaic acid (OA, 1 μM) are positive controls for SIK3 inhibition. Compounds were classified into kinase inhibitors, and uncharacterized compounds, and natural compounds were treated for 36 h at 10 μM, 10 μg/mL, and 50 μg/mL, respectively. Some compounds showed high ratios due to errors, such as cell toxicity. (D) MEF2 and CRTC2 activity were measured in the same GAL4-based firefly luciferase system in the AML-12 cells. (E) Structural activity relationship of pterosin B and its derivatives. HEK293 cells were transformed with the MEF2 or CRTC2 reporter together with the SIK3 expression vector. Compounds (300 μM) were treated for 36 h. n = 2-3.

To visually evaluate the inhibitory actions of pterosin B on SIK3 signaling, green fluoresce protein (GFP)-fusion HDAC5 (a class IIa-HDAC) and CRTC2 were expressed together with SIK3. Both HDAC5 (Fig.1-9A) and CRTC2 (Fig.1-9B) were localized in the cytoplasm in the SIK3-overexpressing cells, and pterosin B inhibited this cytoplasmic localization, suggesting that pterosin B was able to inhibit downstream cascades of SIK3 signaling.

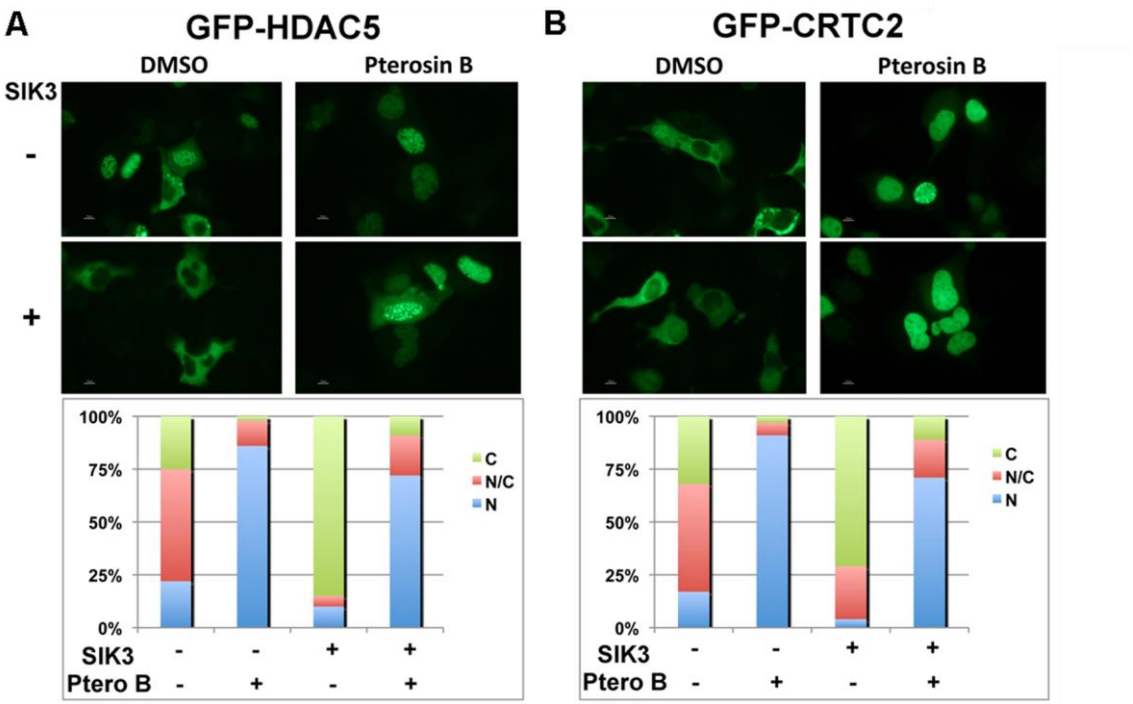

Fig.1-9. Pterosin B inhibits cytoplasmic localization of HDAC5 and CRTC2.
GFP-fusion HDAC5 (A) or CRTC2 (B) were overexpressed in HEK293 cells with or without SIK3 overexpression. Pterosin B (300 μM) was treated for 36 h. The localization of GFP signals in 100 positive cells was classified into three categories, cytoplasmic (C), nucleus (N), and both (C/N) and showed as %.

To examine whether pterosin B inhibits SIK3 signaling and mimics the glucose metabolism observed in SIK3-KO hepatocytes, both WT and SIK3-KO hepatocytes were treated with pterosin B, and glucose production was monitored (Fig.1-10A). Pterosin B quickly increased the medium glucose levels in WT hepatocytes, which was accompanied by enhanced expression of gluconeogenic genes (Fig.1-10B). However, no further enhancement of glucose production or gluconeogenic gene expression by pterosin B was observed in the SIK3-KO hepatocytes, suggesting that pterosin B-induced gluconeogenesis may be mediated by SIK3. Prolonged treatment with pterosin B was found to decrease glucose levels in the WT hepatocyte medium, and *G6pc* gene expression in SIK3-KO hepatocytes was downregulated by pterosin B.

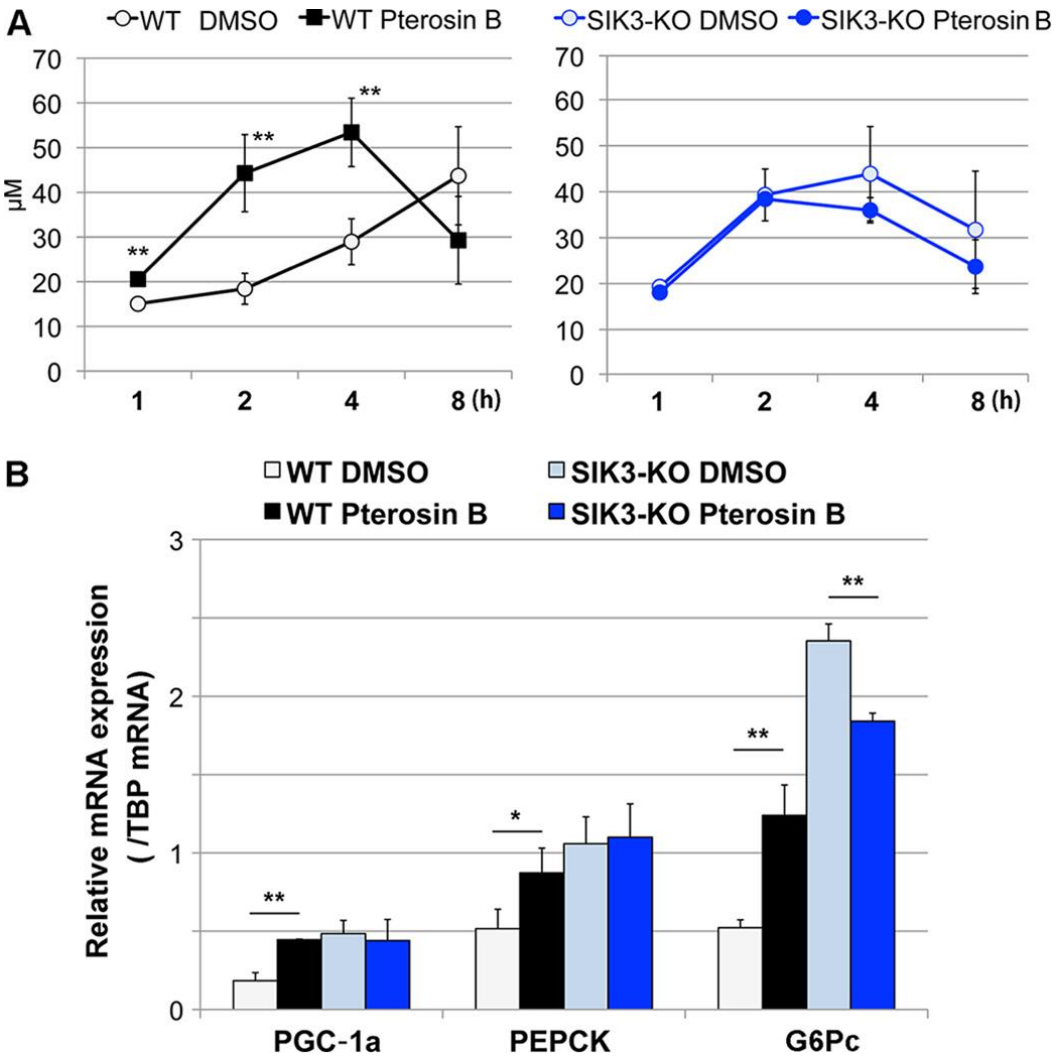

Fig.1-10. Pterosin B upregulates glucose production and gluconeogenic gene expression in WT hepatocytes, but not in SIK3-KO hepatocytes.

(A) Hepatocytes were prepared from 12-week-old female WT (*left panel*) or SIK3-KO (*right panel*) mice (n = 3) and cultured in a low serum (1%) medium for 12 h. The cells were then pretreated with a starvation medium (serum and glucose/glutamate free) for 1 h. Glucose production was induced by 10 mM lactate and 0.1 μM dexamethasone in the presence or absence of pterosin B (300 μM). The means and SD are shown. **, $p < 0.01$.
(B) The hepatocytes were pre-incubated with a low serum (1%) medium for 12 h and incubated in a serum-free medium, a starvation medium alone, or supplemented with pterosin B (300 μM). Total RNA was extracted for qPCR. (n = 3).

1-3. Discussion

SIK3-KO mice display a lean phenotype and excessive hypoglycemia. Although, a response to insulin and lactate-induced gluconeogenesis in SIK3-KO mice appeared to be normal under fasting condition, gluconeogenic gene expression was extremely higher in the SIK3-KO liver than in WT mice. The lean phenotype (small amount of energy storage) can make it difficult to determine whether enhanced gluconeogenic programs in the SIK3-KO mice liver were the results of a cell-autonomous action or systemic effects. Therefore, a role of SIK3 on glucose metabolism in isolated hepatocytes from SIK3-KO mice was examined. SIK3-KO primary hepatocytes produced glucose more quickly after treatment with the cAMP agonist forskolin than the WT hepatocytes, which was accompanied by enhanced gluconeogenic gene expression and CRTC2 dephosphorylation. Pterosin B inhibited SIK3-dependent cytoplasmic localization, suggesting that pterosin B was able to inhibit downstream cascades of SIK3 signaling.

1-4. Reference

1. Takemori, H., and Okamoto, M. (2008) Regulation of CREB-mediated gene expression by salt inducible kinase. *J Steroid Biochem Mol Biol* **108**, 287-291
2. Wang, Z., Takemori, H., Halder, S. K., Nonaka, Y., and Okamoto, M. (1999) Cloning of a novel kinase (SIK) of the SNF1/AMPK family from high salt diet-treated rat adrenal. *FEBS Lett* **453**, 135-139
3. Horike, N., Takemori, H., Katoh, Y., Doi, J., Min, L., Asano, T., Sun, X. J., Yamamoto, H., Kasayama, S., Muraoka, M., Nonaka, Y., and Okamoto, M. (2003) Adipose-specific expression, phosphorylation of Ser794 in insulin receptor substrate-1, and activation in diabetic animals of salt-inducible kinase-2. *J Biol Chem* **278**, 18440-18447
4. Lizcano, J. M., Goransson, O., Toth, R., Deak, M., Morrice, N. A., Boudeau, J., Hawley, S. A., Udd, L., Makela, T. P., Hardie, D. G., and Alessi, D. R. (2004) LKB1 is a master kinase that activates 13 kinases of the AMPK subfamily, including MARK/PAR-1. *Embo J* **23**, 833-843
5. Screaton, R. A., Conkright, M. D., Katoh, Y., Best, J. L., Canettieri, G., Jeffries, S., Guzman, E., Niessen, S., Yates, J. R., 3rd, Takemori, H., Okamoto, M., and Montminy, M. (2004) The CREB coactivator TORC2 functions as a calcium- and cAMP-sensitive coincidence detector. *Cell* **119**, 61-74
6. Berdeaux, R., Goebel, N., Banaszynski, L., Takemori, H., Wandless, T., Shelton, G. D., and Montminy, M. (2007) SIK1 is a class II HDAC kinase that promotes survival of skeletal myocytes. *Nat Med* **13**, 597-603
7. Katoh, Y., Takemori, H., Min, L., Muraoka, M., Doi, J., Horike, N., and Okamoto, M.

(2004) Salt-inducible kinase-1 represses cAMP response element-binding protein activity both in the nucleus and in the cytoplasm. *Eur J Biochem* **271**, 4307-4319

8. Doi, J., Takemori, H., Lin, X.-z., Horike, N., Katoh, Y., and Okamoto, M. (2002) Salt-inducible kinase represses PKA-mediated activation of human cholesterol side chain cleavage cytochrome promoter through the CREB basic leucine zipper domain. *J Biol Chem* **277**, 15629-15637
9. Takemori, H., Katoh, Y., Horike, N., Doi, J., and Okamoto, M. (2002) ACTH-induced nucleocytoplasmic translocation of salt-inducible kinase. Implication in the protein kinase A-activated gene transcription in mouse adrenocortical tumor cells. *J Biol Chem* **277**, 42334-42343.
10. McKinsey, T. A., Zhang, C. L., Lu, J., and Olson, E. N. (2000) Signal-dependent nuclear export of a histone deacetylase regulates muscle differentiation. *Nature* **408**, 106-111
11. Koo, S. H., Flechner, L., Qi, L., Zhang, X., Screaton, R. A., Jeffries, S., Hedrick, S., Xu, W., Boussouar, F., Brindle, P., Takemori, H., and Montminy, M. (2005) The CREB Coactivator TORC2 is a Key Regulator of Fasting Glucose Metabolism. *Nature* **437**, 1109-1111
12. Imai, E., Miner, J. N., Mitchell, J. A., Yamamoto, K. R., and Granner, D. K. (1993) Glucocorticoid receptor-cAMP response element-binding protein interaction and the response of the phosphoenolpyruvate carboxykinase gene to glucocorticoids. *J Biol Chem* **268**, 5353-5356
13. Bertorello, A. M., Pires, N. M., Igreja, B., Pinho, M. J., Vorkapic, E., Wagsater, D., Wikstrom, J., Behrendt, M., Hamsten, A., Eriksson, P., Soares-da-Silva, P., and Brion, L. (2015) Increased Arterial Blood Pressure and Vascular Remodeling in

Mice Lacking Salt-Inducible Kinase 1 (SIK1). *Circ Res*

14. Muraoka, M., Fukushima, A., Viengchareun, S., Lombes, M., Kishi, F., Miyauchi, A., Kanematsu, M., Doi, J., Kajimura, J., Nakai, R., Uebi, T., Okamoto, M., and Takemori, H. (2009) Involvement of SIK2/TORC2 signaling cascade in the regulation of insulin-induced PGC-1alpha and UCP-1 gene expression in brown adipocytes. *Am J Physiol Endocrinol Metab* **296**, E1430-1439
15. Horike, N., Kumagai, A., Shimono, Y., Onishi, T., Itoh, Y., Sasaki, T., Kitagawa, K., Hatano, O., Takagi, H., Susumu, T., Teraoka, H., Kusano, K., Nagaoka, Y., Kawahara, H., and Takemori, H. (2010) Downregulation of SIK2 expression promotes the melanogenic program in mice. *Pigment Cell Melanoma Res* **23**, 809-819
16. Park, J., Yoon, Y. S., Han, H. S., Kim, Y. H., Ogawa, Y., Park, K. G., Lee, C. H., Kim, S. T., and Koo, S. H. (2014) SIK2 is critical in the regulation of lipid homeostasis and adipogenesis in vivo. *Diabetes* **63**, 3659-3673
17. Sakamaki, J., Fu, A., Reeks, C., Baird, S., Depatie, C., Al Azzabi, M., Bardeesy, N., Gingras, A. C., Yee, S. P., and Screaton, R. A. (2014) Role of the SIK2-p35-PJA2 complex in pancreatic beta-cell functional compensation. *Nat Cell Biol* **16**, 234-244
18. Inagaki T, Dutchak P, Zhao G, Ding X, Gautron L, Parameswara V, Li Y, Goetz R, Mohammadi M, Esser V, Elmquist JK, Gerard RD, Burgess SC, Hammer RE, Mangelsdorf DJ & Kliewer SA (2007) Endocrine regulation of the fasting response by PPARalpha-mediated induction of fibroblast growth factor 21. *Cell Metab* **5**, 415-425.
19. Mihaylova MM, Vasquez DS, Ravnskjaer K, Denechaud PD, Yu RT, et al.(2011) Class IIa Histone Deacetylases Are Hormone-Activated Regulators of FOXO and

Mammalian Glucose Homeostasis. Cell 145: 607–621.

20. Takemori H, Katoh-Hashimoto Y, Nakae J, Olson EN, Okamoto M (2009) Inactivation of HDAC5 by SIK1 in AICAR-treated C2C12 myoblasts. Endocr J 56: 121–130.

21. Katoh, Y., Takemori, H., Lin, X. Z., Tamura, M., Muraoka, M., Satoh, T., Tsuchiya, Y., Min, L., Doi, J., Miyauchi, A., Witters, L. A., Nakamura, H., and Okamoto, M. (2006) Silencing the constitutive active transcription factor CREB by the LKB1-SIK signaling cascade. *Febs J* **273**, 2730-2748

22. Walkinshaw, D. R., Weist, R., Kim, G. W., You, L., Xiao, L., Nie, J., Li, C. S., Zhao, S., Xu, M., and Yang, X. J. (2013) The tumor suppressor kinase LKB1 activates the downstream kinases SIK2 and SIK3 to stimulate nuclear export of class IIa histone deacetylases. *J Biol Chem* **288**, 9345-9362

23. Kumagai, A., Horike, N., Satoh, Y., Uebi, T., Sasaki, T., Itoh, Y., Hirata, Y., Uchio-Yamada, K., Kitagawa, K., Uesato, S., Kawahara, H., Takemori, H., and Nagaoka, Y. (2011) A Potent Inhibitor of SIK2, 3, 3', 7-Trihydroxy-4'-Methoxyflavon (4'-O-Methylfisetin), Promotes Melanogenesis in B16F10 Melanoma Cells. *PLoS One* **6**, e26148

CHAPTER2

Pterosin B regulates hepatic gluconeogenesis via a SIK3-dependent mechanism.

2-1. Introduction

In the chapter2, the relation between pterosin B and SIK3 signal in respect to hepatic gluconeogenesis is described.

2-2. Results

Pterosin B represses SIK3 signaling via the C-terminal regulatory region

To test the specificity of pterosin B toward SIKs, SIK1-3 was examined in the same reporter assay in the HEK293 cells (Fig.2-1A). The upregulation of MEF2 and downregulation of CRTC2 activities by SIK1 or SIK2 were not affected by pterosin B, indicating that pterosin B specifically inhibited SIK3 signaling. On the other hand, pterosin B did not inhibit SIK3 kinase activity up to 1 mM, while the strong pan-SIK inhibitor HG9-91-01 (1) completely inhibited SIK3 kinase activity even at 1 μM (Fig. 2-1B). Because SIK3 was activated by phosphorylation at Thr163 by the upstream kinase LKB1 (2), the phosphorylation status at this site on the overexpressed SIK3 in HEK293 cells was examined (Fig.2-1C). Western blot analyses with anti-phospho-Thr163 revealed that pterosin B did not alter the phosphorylation level at this site. The alternative candidate sites for inhibition of the SIK3 actions were in the

C-terminal regulatory domains of Thr411 and Ser493 (Fig.2-1D) (3). The phosphorylation of these sites suppressed SIK3's CRTC-inhibitory activity. To confirm the importance of the C-terminal domain, reporter assays with various SIK3 mutants were used. The truncation of the C-terminal domain (kinase domain only) converted SIK3 into a pterosin B-resistant mutant (Fig.2-1D). The actions of double mutant SIK3 (DA: T411A and S493A) were also not affected by pterosin B (Fig.2-1E), despite a small difference between the MEF2 and CRTC2 systems (Thr411 may be more critical for CRTC2 regulation than Ser493). Indeed, the phosphorylation levels at Thr411 and Ser493 were upregulated in mouse hepatoma AML-12 cells treated with pterosin B, which was also found in Fsk-treated cells (Fig.2-2A). Ser493 may be phosphorylated by PKA (4), and overexpression of PKA in HEK293 cells mimicked the pterosin actions on MEF2 and CRTC2 (Fig.2-2B). However, the PKA inhibitor H89 did not block pterosin B-dependent suppression of SIK3 signaling (Fig.2-2C). Although Thr411 is probably phosphorylated by PKA or CaMKs, the overexpression of CaMK I/II or the treatment with the CaMK inhibitor KN62 disproved the involvement of these kinases in the pterosin B-dependent suppression of SIK3 signaling (Figs.2-2B and 2-2C). In addition, the cAMP-responsible luciferase system showed that pterosin B reduced the intracellular cAMP levels induced by Fsk (Fig.2-2D). These results suggested that unknown kinases, rather than PKA or CaMK I/II, might phosphorylate SIK3 in Thr411 and Ser491, which inhibited SIK3 signaling.

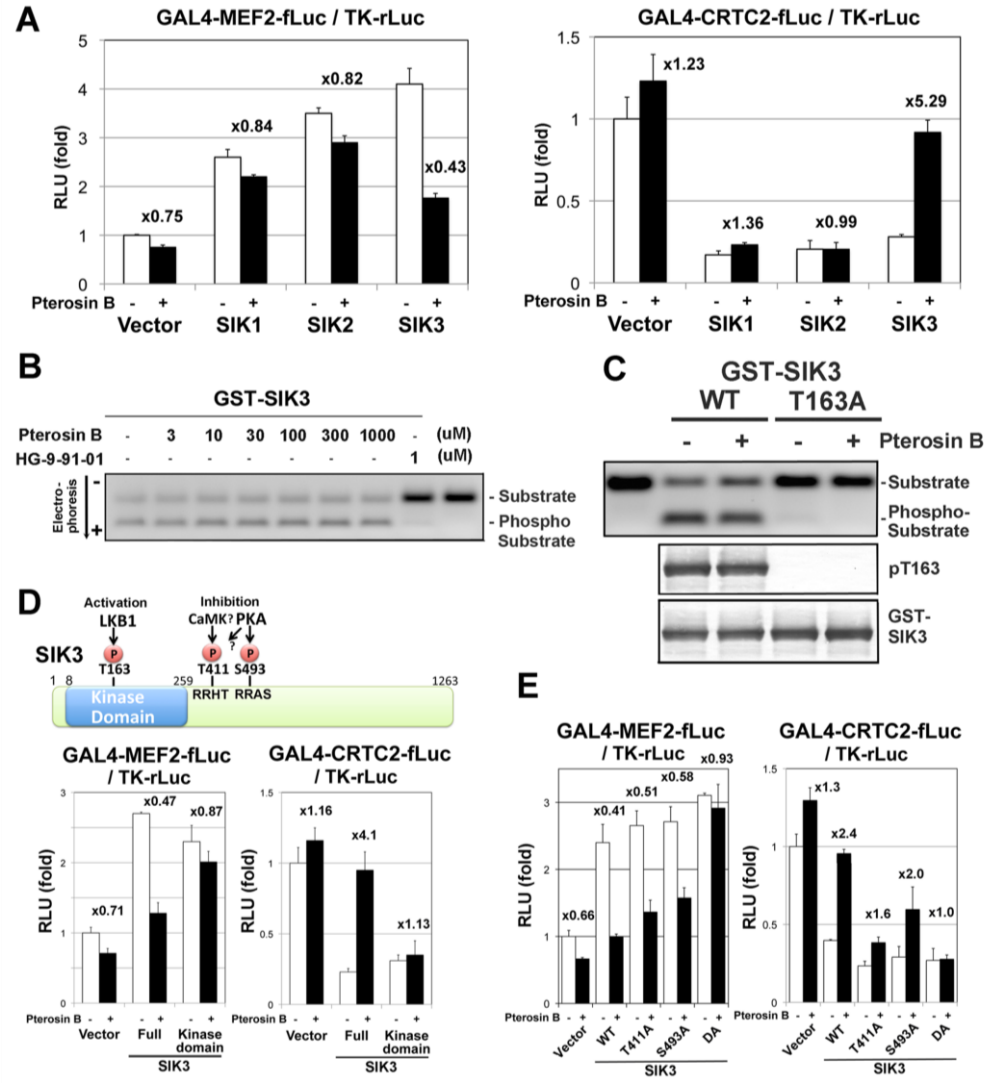

Fig.2-1. Pterosin B represses SIK3 signaling via the C-terminal regulatory region.

(A) HEK293 cells were transformed with the MEF2 or CRTC2 reporter together with the SIK1-3 expression vectors and treated with pterosin B (300 μM) for 36 h. The fold differences in the reporter activities by the pterosin B treatment were indicated (n = 3, Means and SD.). (B) *In vitro* kinase assay. The GST-SIK3 enzyme was expressed in HEK293 cells, purified with a glutathione resin and incubated with compounds, the coumarin-labeled CRTC2 peptide, and 1 mM ATP for 1 h. The phosphorylated and non-phosphorylated peptides were separated by electrophoresis. (C) HEK293 cells overexpressing GST-SIK3 (WT and T163A mutant) were treated with pterosin B (300 μM) for 36 h, and then the GST-SIK3 were purified and subjected to the *in vitro* kinase assay and western blot analysis. (D) Upper diagram shows phosphorylation sites in SIK3. HEK293 cells were transformed with reporters together with the SIK3 expression vectors as (A). (E) The same experiments with SIK3-phoshorylation site mutants were performed.

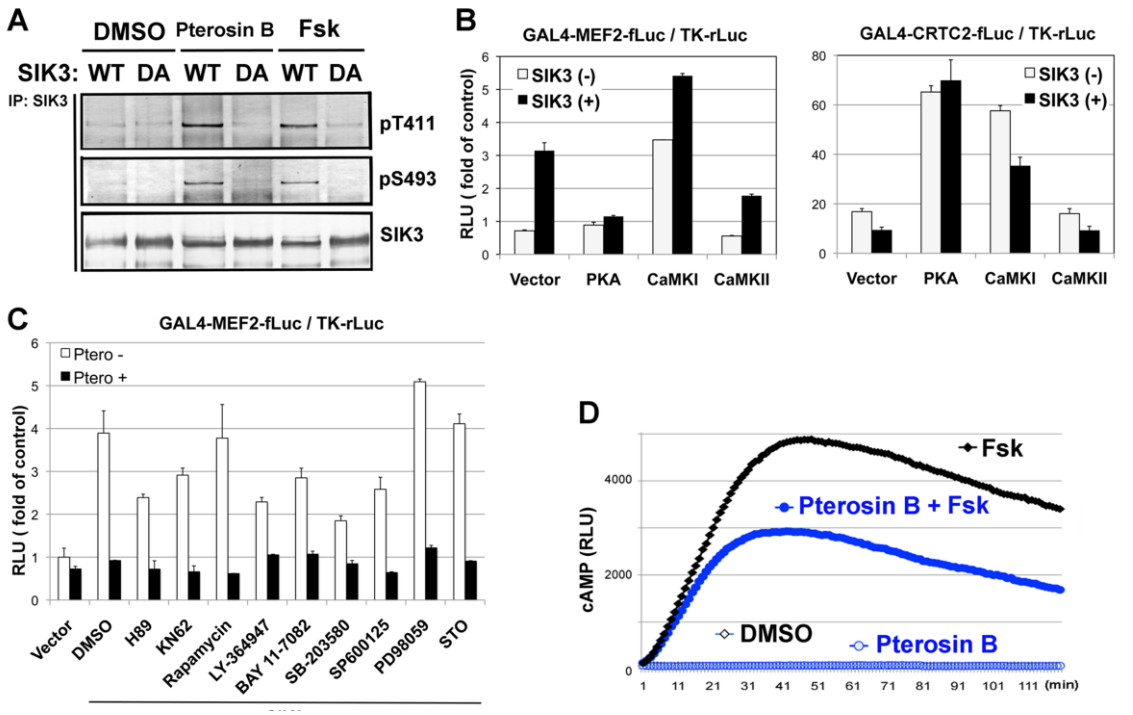

Fig.2-2. PKA or CaMKs is not responsible kinase for the pterosin B-mediated suppression of SIK3 signaling.

(A) AML-12 cells were transfected with SIK3 (WT and DA mutant) adenoviruses and were treated with pterosin B (300 μM) or Fsk (20 μM). Three hours later, SIK3 protein was purified with anti-SIK3 antibodies and subjected to western blot analyses. (B) HEK293 cells were transformed with the MEF2 or CRTC2 reporter together with the SIK3 and PKA or CaMK I/II expression vector. Luciferase activities were measured after 36 h. n=3. (C) Effects of various inhibitors on pterosin B-mediated suppression of SIK3-dependent MEF2C activity. H89 (20 μM, PKA inhibitor), KN62 (10 μM, CaMK inhibitor), Rapamycin (1μM, PI3K/Akt/mTOR signal inhibitor), LY364947 (10 μM, TGF-β receptor inhibitor), BAY 11-7082 (10 μM, IKK inhibitor), SB-203580 (10 μM, p38 inhibitor), SP600125 (10 μM, JNK inhibitor), PD98059 (10 μM, MEK inhibitor), and STO609 (30 μM, CaMKK inhibitor) were used. (D) AML-12 cells that had been transformed with the cAMP sensor plasmid GloSensor™ were treated with Fsk (20 μM) together with or without pterosin B (300 μM). The cellular cAMP level was monitored as luciferase activities.

Pterosin B-resistant SIK3 decreases glucose production and CRTC2 dephosphorylation in AML-12 cells

To specifically examine the signaling in pterosin B-induced gluconeogenesis and the relevance of the importance of the C-terminal domain of SIK3, glucose production in AML-12 cells after pterosin B treatment was examined. Pterosin B increased glucose production as quickly as Fsk, while HG9-91-01 increased it gradually (Fig.2-3A). At 8 h post-stimulation, however, the glucose level in pterosin B-treated cells was returned to the basal level. Because the higher potential of pterosin B on glucose production than HG9-91-01 suggested the presence of SIK-independent pathways in pterosin B actions, pterosin B-induced glucose production in the AML-12 cells that had been transfected with SIK3-adenoviruses was examined. Overexpression of SIK3 lowered the pterosin B-induced glucose production, which was more evident in cells that expressed pterosin B-resistant SIK3 DA mutant than in pterosin B-sensitive SIK3 (WT) (Fig.2-3B). Next, The levels of gluconeogenic gene expression in the pterosin B-treated AML-12 cells was examined. Cells were pretreated with serum-free medium for 1 h and then, incubated with pterosin B or other compounds in the absence of glucose for 3 h. Pterosin B upregulated *Pgc1a*, *Pepeck,* and *G6pc* mRNA levels with different efficacies, which was also represented by Fsk and HG9-91-01 with different target specificities (Fig.2-3C). Again, it was examined whether SIK3 overexpression was able to suppress pterosin B-induced gluconeogenic gene expressions. All expressions were suppressed by SIK3 overexpression, and SIK3 DA was more efficient than SIK WT (Fig.2-3D). Then, the protein status involved in gluconeogenesis was examined. Pterosin B quickly induced the dephosphorylation of CRTC2 in AML-12 cells (Fig.2-3E), which was also observed in Fsk- and HG9-91-01-treated cells. CREB phosphorylation at Ser133 was

upregulated with starvation time in the control (DMSO) cells. However, the treatment with pterosin B or HG9-91-01 inhibited the CREB phosphorylation. An increase in AMPK phosphorylation levels at Thr172 was further upregulated in pterosin B-treated cells and downregulated in Fsk-treated cells. HG9-91-01 apparently showed no effect on the AMPK phosphorylation levels. Similarly to other assays, SIK3 overexpression returned the levels of pterosin B-induced dephosphorylation of CRTC2 and phosphorylation of CREB (Fig.2-3F), which was, again, more evidently with SIK3 DA than SIK3 WT. These results suggested that dephosphorylation of CRTC2 by pterosin B might induce gluconeogenic programs, and the inactivation of SIK3 due to enhanced phosphorylation of its C-terminal domain might be a mechanism of these programs.

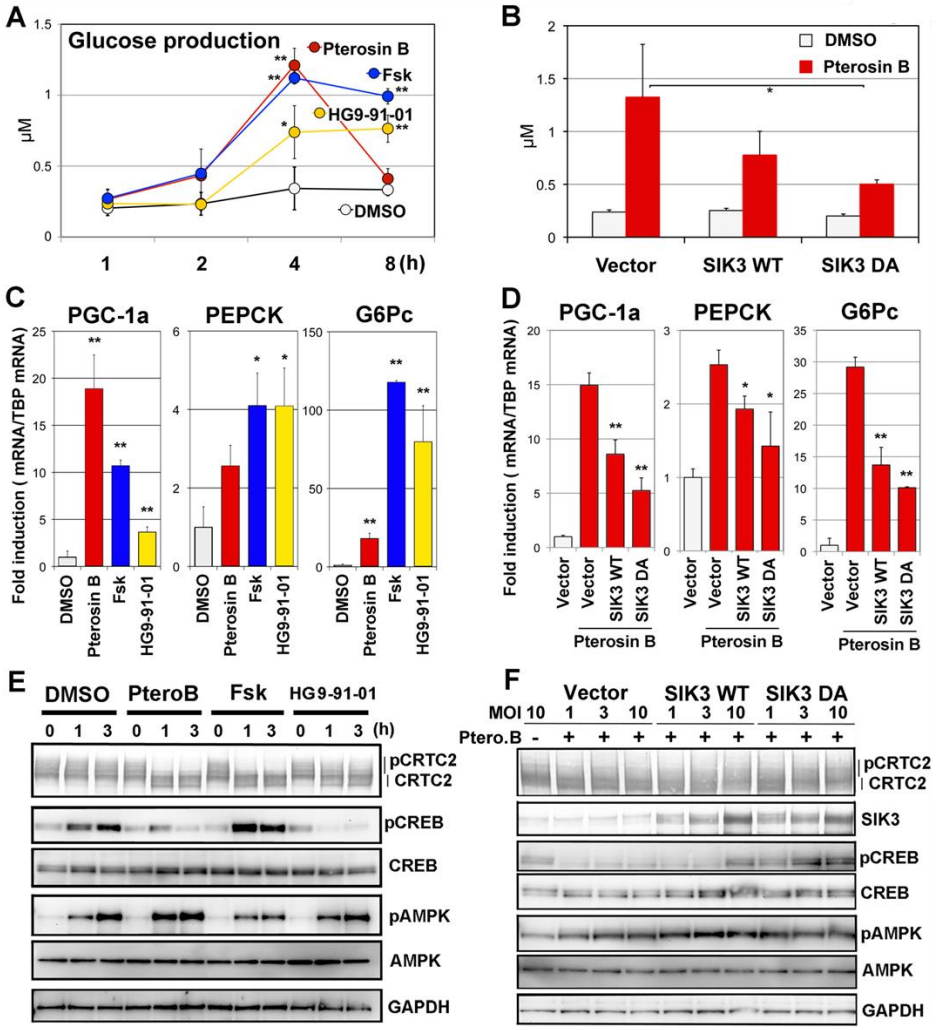

Fig.2-3. Pterosin B resistant SIK3 suppresses pterosin B induced gluconeogenic programs.

(A) AML-12 cells that had been incubated in 1% serum medium for 12 h were further pre-incubated with the starvation medium (serum- and glucose-/glutamate-free) for 1 h. Means and SD were indicated (n = 4). *, $p < 0.05$; **, $p < 0.01$ (compared with the control group, DMSO). Glucose production was induced by pterosin B (300 μM), Fsk (20 μM), or HG9-91-01 (1 μM) in the presence of 10 mM lactate and 0.1 μM dexamethasone. (B) AML-12 cells that had been transfected with the SIK3 (WT and DA mutant) adenoviruses were subjected to glucose production assays (at 3 h). *, $p< 0.05$ (compared with the control pterosin B group, Vector) (C) Gluconeogenic mRNA were examined in the AML-12 cells. Cells that were incubated with a serum-free medium for 12 h and treated with compounds (same as A) in the starvation medium for 3 h (n = 3). (D) The pterosin B-induced gene expression was analyzed in the SIK3-overexpressing AML-12 cells. E. Western blot analyses of AML-12 cells that were treated as in C. F. The pterosin B treatment was for 3 h. MOI, multiplicity of infection.

Involvement of PHKG2 in pterosin B-mediated inactivation of SIK3

Finally, the molecules mediating pterosin B action on SIK3 were identified, which could be a kinase or a phosphatase. Some candidates were overexpressed in the MEF2 and CRTC2 reporter systems in HEK293 cells, and SIK3-dependent activation and repression were evaluated in the presence or absence of pterosin B (Fig.2-4A). It has been reported that the phosphatases PP1, PP2A, and calcineurin (Cn) modulate CRTC2 activity (5). However, these phosphatases modulate reporter activities of either MEF2 or CRTC2. Pyruvate dehydrogenase kinase (PDK) and pyruvate dehydrogenase phosphatase (PDP) are key regulators in mitochondria and regulate acetyl-CoA production by modulating pyruvate dehydrogenase (PDH) activity (6). PDH activity is inextricably linked with pyruvate carboxylase, producing oxaloacetic acid, which is the initial metabolite of gluconeogenesis. However, PDK(s) and PDP(s) did not modulate SIK3-dependent MEF2 or CRTC2 activities. When gluconeogenesis is activated in hepatocytes, glycogenolysis could also be activated. The key molecules regulating glycogenolysis are phosphorylases and are activated by phosphorylase kinase catalytic gamma 2 (PHKG2). Indeed, PHKG2, but no the muscle type PHKG1, inhibited the SIK3-dependent regulation of both MEF2 and CRTC2, which is accelerated by pterosin B (when SIK3 is inhibited, the fold change approaches 1). In addition, 3 h of treatment with pterosin B decreased the glycogen content in AML-12 cells in a dose-dependent manner (Fig.2-4B), suggesting that pterosin B stimulates glycogenolysis.

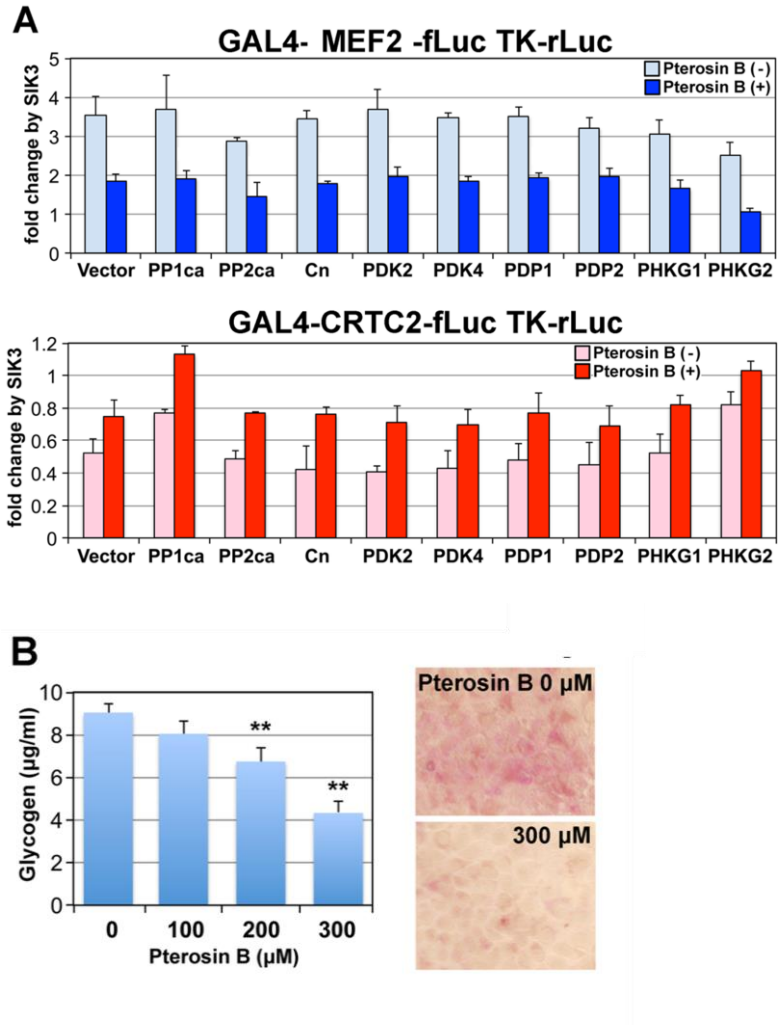

Fig.2-4. PHKG2 inactivates SIK3 in response to pterosin B.

(A) A reporter assay was performed in HEK293 cells. Some kinases and phosphatases were overexpressed together with GAL4-MEF2 or GAL4-CRTC2 reporters (see FIGURE 2B). Bars indicate fold activation (MEF2) or repression (CRTC2) by SIK3 overexpression (n = 3). In SIK3 without transcriptional regulatory activity, the fold change (activation or repression) approaches 1 (no change). Pterosin B was added at 300 μM. (B) AML-12 cells that had been cultured for 72 h with daily medium change were incubated with various concentrations of pterosin B (0–300 μM) for 3 h. The glycogen concentrations were then measured (*left panel*). Intracellular accumulation of glycogen was observed after PAS staining (*right panel*).

An *in vitro* kinase assay of PHKG2 and SIK3 peptide corresponding to the regions of Thr411 and Ser493 indicates that PHKG2 can phosphorylate SIK3 (Fig.2-5A). GST pull-down in AML-12 cells suggests that PHKG2 binds to SIK3 in response to pterosin B (Fig.2-5B) in a T411- or S493-phosphorylation-independent manner (Fig.2-5C). The association with PHKG2 was only observed when SIK3 was used as bait (Fig.2-5D). On the other hand, the overexpression of PHKG2 in AML-12 cells had less of an effect on the SIK3 cascades downstream, probably because of the limited amount of SIK3 protein.

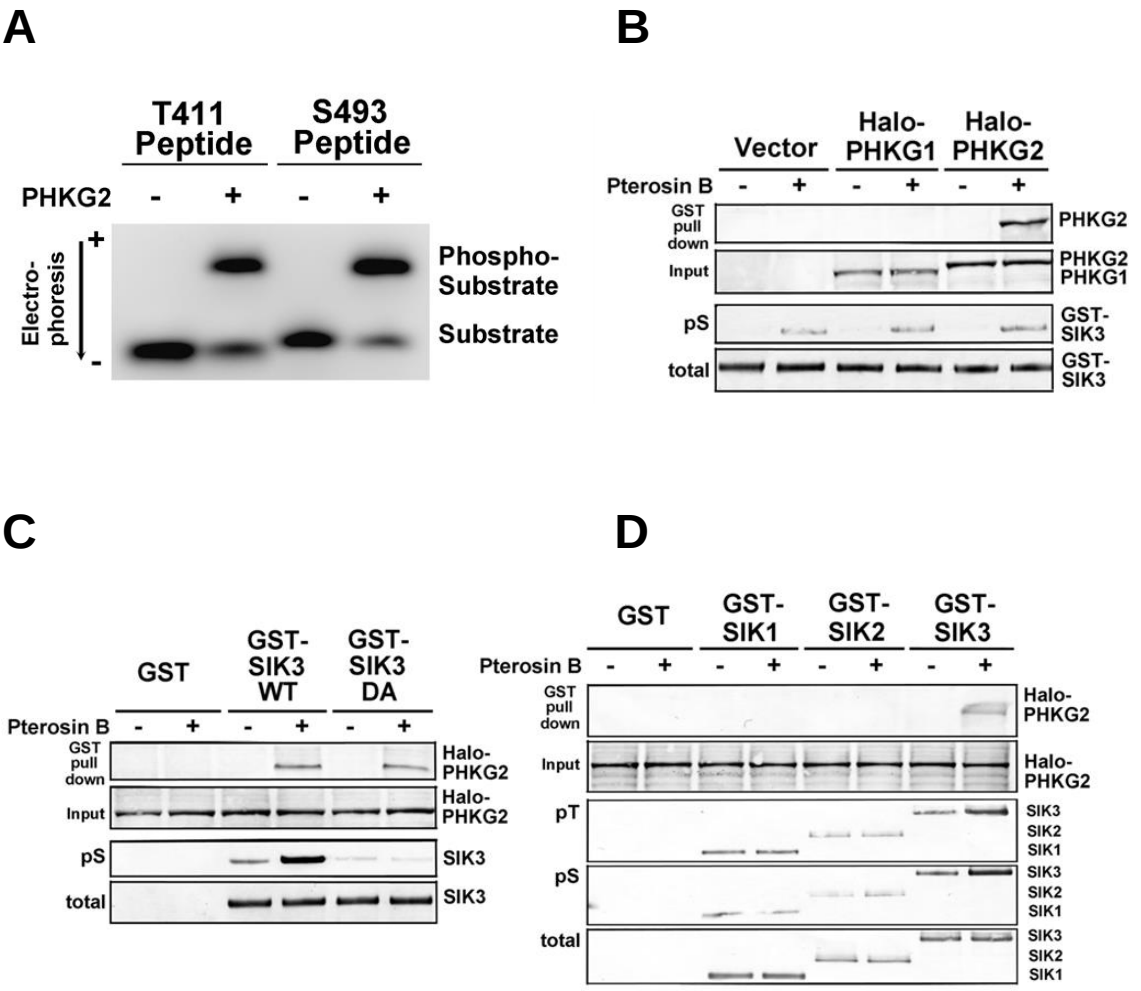

Fig.2-5. PHKG2 inactivates SIK3 in response to pterosin B.

(A) The GST-fusion PHKG2 enzyme was overexpressed in COS-7 cells and purified using glutathione column. Fluoro-peptides corresponding to SIK3 Thr411 and Ser493 were incubated with GST-PHKG2 in the presence of ATP. Phosphorylated peptides were separated by electrophoresis on agarose gel. (B) GST-SIK3 were overexpressed in AML-12 cells in the presence of Halo-tagged PHKG1/2 and pull-down by glutathione sepharose after 3 h of pre-treatment with pterosin B (300 μM). PHKG1/2 and phospho-SIK3 (pS) were detected by anti-Halo-tag antibody and anti-pS493, respectively. (C) GST-SIK3 WT and T411A/S493A mutant (DA) were used. (D) GST SIK1-3 were used.

To show the indispensable role of PHKG2 in pterosin B-mediated SIK3 inactivation, knockdown experiments were performed in AML-12 cells. Two different miRNA vectors for mouse PHKG2 decreased the protein levels and lowered the phosphorylation levels of SIK3 pT411 and pS493 (Fig.2-6A), in contrast to CRTC2 phosphorylation levels. Pterosin B-induced gluconeogenic gene expression was also suppressed by PHKG2 knockdown (Fig.2-6B), suggesting that PHKG2 is a new regulator of SIK3 as elicited by pterosin B.

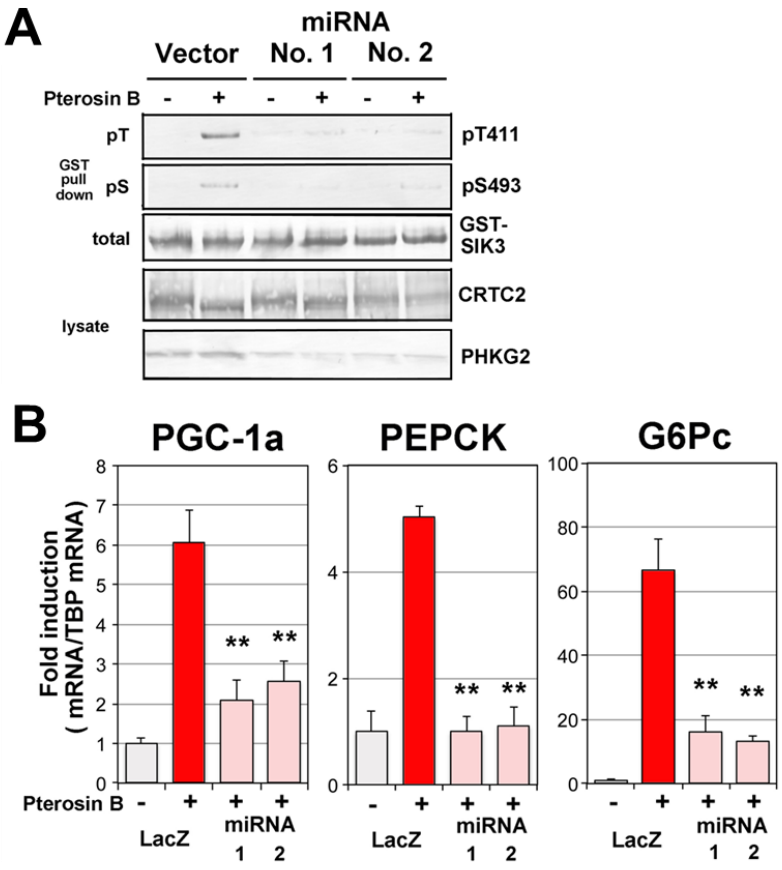

Fig.2-6. PHKG2 inactivates SIK3 in response to pterosin B.

(A) PHKG2 protein was knocked down in AML-12 cells by transformation with miRNA plasmid vectors. (B) The same sequences of miRNA were transferred into an adenovirus vector and knocked down PHKG2 protein in AML-12 cells to monitor pterosin B-induced gluconeogenic gene expression (300 μM, 2 h). n = 3, **, $p < 0.01$ (compared with the control group, LacZ - pterosin B).

2-3. Discussion

In this chapter, it has been demonstrated that pterosin B suppressed SIK3 downstream cascades by up-regulating the phosphorylation levels in the SIK3 C-terminal regulatory domain. When pterosin B promoted glucose production by up-regulating gluconeogenic gene expression in AML-12 cells, it decreased the glycogen content and stimulated an association between PHKG2 and SIK3. PHKG2 phosphorylated the peptides with sequences of the C-terminal domain of SIK3.

PHKG2 belongs to the CaMK family (7) and shares phosphorylation motifs with CaMKs and PKA (8). A major role of PHKG2 is the initiation of glycogen breakdown in response to glucagon-cAMP-PKA or Ca2+ signaling by phosphorylating phosphorylase (9). Mutations in the *PHKG2* gene cause type IXc glycogen storage disease (GSD: liver glycogenosis), which is characterized by hypoglycemia, lactic acidosis, and cirrhosis (10). Although glucagon response was found in type IX GSD patients (11), some patients with *PHKG2* gene mutations were reported to not or weakly respond to glucagon (12). In addition, Type Ia GSD, G6Pc deficiency (13), and PEPCK deficiency (liver isoform PCK1) (14)commonly cause lactic acidosis, suggesting the dysregulation of gluconeogenesis in *PHKG2*-mutated patients. A decrease in the glycogen content in pterosin B-treated AML-12 cells, capability of SIK3 phosphorylation by PHKG2 *in vitro*, specific association of PHKG2 with SIK3, and weakened action of pterosin B in PHKG2 knocked-down AML-12 suggest that pterosin B inactivates SIK3 via the activation of PHKG2. These results suggest that pterosin B suppress SIK3 via PHKG2.

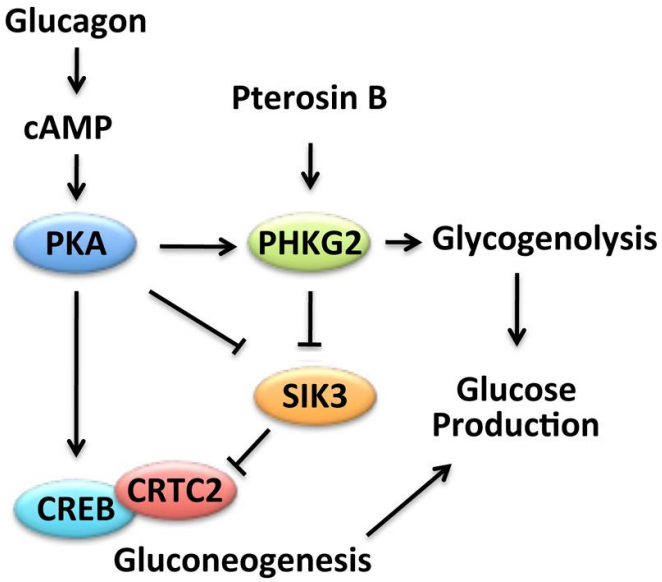

Fig.2-7. Hypothetical model of SIK3 signaling.

2-4. Reference

1. Clark, K., MacKenzie, K. F., Petkevicius, K., Kristariyanto, Y., Zhang, J., Choi, H. G., Peggie, M., Plater, L., Pedrioli, P. G., McIver, E., Gray, N. S., Arthur, J. S., and Cohen, P. (2012) Phosphorylation of CRTC3 by the salt-inducible kinases controls the interconversion of classically activated and regulatory macrophages. *Proc Natl Acad Sci U S A* **109**, 16986-16991

2, Lizcano, J. M., Goransson, O., Toth, R., Deak, M., Morrice, N. A., Boudeau, J., Hawley, S. A., Udd, L., Makela, T. P., Hardie, D. G., and Alessi, D. R. (2004) LKB1 is a master kinase that activates 13 kinases of the AMPK subfamily, including MARK/PAR-1. *Embo J* **23**, 833-843

3. Sasaki, T., Takemori, H., Yagita, Y., Terasaki, Y., Uebi, T., Horike, N., Takagi, H., Susumu, T., Teraoka, H., Kusano, K., Hatano, O., Oyama, N., Sugiyama, Y., Sakoda, S., and Kitagawa, K. (2011) SIK2 is a key regulator for neuronal survival after ischemia via TORC1-CREB. *Neuron* **69**, 106-119

4. Takemori, H., and Okamoto, M. (2008) Regulation of CREB-mediated gene expression by salt inducible kinase. *J Steroid Biochem Mol Biol* **108**, 287-291

5. Uebi, T., Tamura, M., Horike, N., Hashimoto, Y. K., and Takemori, H. (2010) Phosphorylation of the CREB-specific coactivator TORC2 at Ser(307) regulates its intracellular localization in COS-7 cells and in the mouse liver. *Am J Physiol Endocrinol Metab* **299**, E413-425

6. Zhang, S., Hulver, M. W., McMillan, R. P., Cline, M. A., and Gilbert, E. R. (2014) The pivotal role of pyruvate dehydrogenase kinases in metabolic flexibility. *Nutr Metab (Lond)* **11**, 10

7. Hanks, S. K. (1987) Homology probing: identification of cDNA clones encoding members of the protein-serine kinase family. *Proc Natl Acad Sci U S A* **84**, 388-392

8. Chan, K. F., Hurst, M. O., and Graves, D. J. (1982) Phosphorylase kinase specificity. A comparative study with cAMP-dependent protein kinase on synthetic peptides and peptide analogs of glycogen synthase and phosphorylase. *J Biol Chem* **257**, 3655-3659

9. Chrisman, T. D., and Exton, J. H. (1980) Activation of endogenous phosphorylase kinase in liver glycogen pellet by cAMP-dependent protein kinase. *J Biol Chem* **255**, 3270-3273

10. Maichele, A. J., Burwinkel, B., Maire, I., Sovik, O., and Kilimann, M. W. (1996) Mutations in the testis/liver isoform of the phosphorylase kinase gamma subunit (PHKG2) cause autosomal liver glycogenosis in the gsd rat and in humans. *Nat Genet* **14**, 337-340

11. Dunger, D. B., and Leonard, J. V. (1982) Value of the glucagon test in screening for hepatic glycogen storage disease. *Arch Dis Child* **57**, 384-389

12. Burwinkel, B., Rootwelt, T., Kvittingen, E. A., Chakraborty, P. K., and Kilimann, M. W. (2003) Severe phenotype of phosphorylase kinase-deficient liver glycogenosis with mutations in the PHKG2 gene. *Pediatr Res* **54**, 834-839

13. Oei, T. L. (1962) Hexose monophosphate, pyruvate and lactate in the peripheral blood in glycogen-storage disease type I. *Clin Chim Acta* **7**, 193-198

14. Haworth, J. C., Robinson, B. H., and Perry, T. L. (1981) Lactic acidosis due to pyruvate carboxylase deficiency. *J Inherit Metab Dis* **4**, 57-58

CHAPTER 3

Pterosin B regulates hepatic gluconeogenesis via a SIK3-independent mechanism.

3-1. Introduction

Hsu et al., (1) had reported that pterosin A (a derivative of pterosin B) lowered blood glucose levels and hepatic *Pck1* expression in mice, coupled with AMPK activation. In addition, our study in chapter 3 also found that the magnitude of pterosin B-induced *G6pc* gene expression was much lower than that induced by forskolin (a cAMP-agonist) in mouse hepatoma cell line, AML-12, suggesting that pterosin B (probably pterosin A as well) affects gluconeogenic gene expression at multiple sites and not only at the SIK3-CRTC2 cascade.

The retinoic acid receptor-related orphan receptor (ROR) family of transcription factors is composed of three isoforms (α, β, and γ), which play important roles in a variety of physiological events, including glucose and lipid metabolism, development of immune- and neural-systems, and circadian rhythms (2,3). In this family, RORα has been found to be regulated by cAMP signaling (4). Studies using knockout models and specific ligands of RORα suggested a participation of this transcription factor in the regulation of gluconeogenesis (5,6). Steroid receptor coactivator 2 (SRC2) activates RORα on the *G6pc* promoter, and the deficiency in either RORα or SRC2 shares phenotypes (hypoglycemia and excess glycogen storage) with G6Pc deficiency, which is classified as glycogen storage disease type 1a (Von Gierke's Disease) (5,7).

In this chapter, a new regulation site of pterosin B via a SIK3 -independent mechanism

is described.

3-2. Results

Suppress forskolin-dependent hepatic glucose production

Since pterosin A, a derivative of pterosin B, has anti-diabetic effects in streptozotocin-treated mice and *db/db* mice (1), *db/db* mice were fed with a diet containing pterosin B. Like pterosin A, an 1-month treatment with pterosin B also lowered blood glucose levels and enhanced insulin responses in these mice (Fig.3-1B).

Although pterosin B has the potential to promote gluconeogenic gene expression via CRTC2 activation, the glucose production induced by it lasted for only several hours in the AML-12 cel. Thus, the glucose production in mouse hepatocytes stimulated with pterosin B, forskolin, and their combination was re-evaluated. Although pterosin B and forskolin synergistically upregulated glucose production at 1 h post stimulation (Fig.3-1C), pterosin B acted as a suppressor of forskolin-dependent glucose production in later phases (4 h).

Synergistic or additive induction by pterosin B and forskolin was observed in *Ppargc1a* and *Pck1* mRNA expression (Fig.3-1D). Although *G6pc* expression was upregulated by pterosin B, the magnitude was much less than that induced by forskolin. Moreover, forskolin-induced *G6pc* gene expression was strongly suppressed by co-treatment with pterosin B. These results suggest that pterosin B alone had the potential to promote gluconeogenic programs; however, in the cAMP cascades, it might act as a suppressor of gluconeogenesis by inhibiting *G6pc* expression.

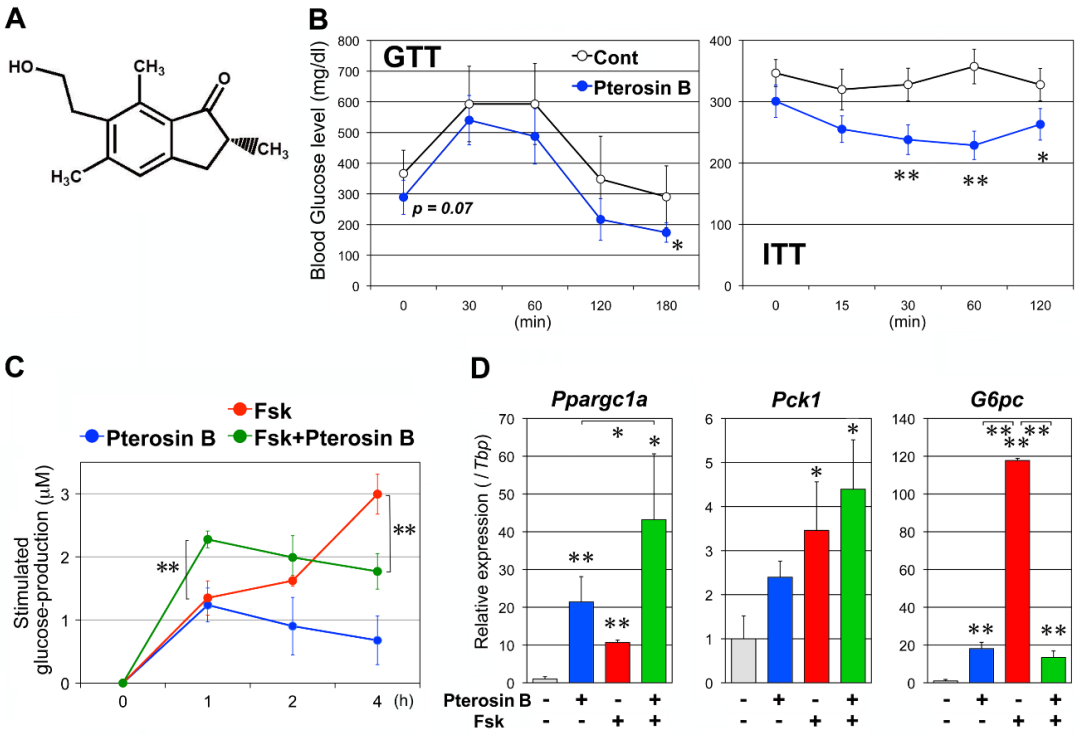

Fig.3-1. Pterosin B lowers blood glucose levels in *db/db* mice

(A) Pterosin B structure. (B) *db/db* mice (10-week-old males, n = 6) that had been fed with diets (chow ± pterosin B, 0.1%: approximately 100 mg/kg/day) for 1 month were subjected to glucose tolerance test (GTT: 1.5 g/kg glucose) or insulin (ITT: 36 μg/kg insulin) tolerance test. Means and s.d. are shown. *: $p < 0.05$, **: $p < 0.01$. (C) Mouse hepatocytes (C57BL/6J) were incubated with 1 mM pyruvate and 10 mM lactate, and glucose production was stimulated with pterosin B (300 μM), forskolin (10 μM), or their combination. The culture media were collected to measure glucose at 1, 2, 4, and 8 h, and "stimulated glucose-production" was calculated by subtraction of glucose levels in control groups (DMSO) from those in individual stimulant groups (n = 4). (D) Mouse hepatocytes (n = 3) had been pre-incubated in the DMEM medium supplemented with 2.5 mM glucose (pyruvate and glutamine free) for 1 h and then treated with pterosin B (300 μM) or forskolin (10 μM) for 2 h. The mRNA expressions of gluconeogenic genes were measured by quantitative PCR. The level of each mRNA was normalized by that of *Tbp* (TATA-box binding protein).

Pterosin B inhibits RORα-SRC2 interaction

Results from previous reports suggest that the loss of the *Src2* gene in mouse hepatocytes results in a lowered *G6pc* expression without affecting *Pck1* expression (5). Because SRC2 is recruited to RORα on the *G6pc* gene promoter, whether pterosin B targeted RORα–SRC2 was tested. Pterosin B alone upregulated *G6pc* promoter activity and downregulated forskolin-dependent *G6pc* promoter activity in AML-12 cells (Fig. 3-2A). Once the ROR-response element was disrupted, pterosin B-dependent suppression of the forskolin-induced *G6pc* promoter activity was not observed. Curiously, although RORα overexpression resulted in a significant enhancement of the wild type *G6pc* promoter activity (Fig.3-2B), pterosin B failed to modulate this activity. On the other hand, pterosin B suppressed SRC2-induced *G6pc* promoter activity, suggesting that SRC2 might be the major target of pterosin B, and RORα might be transmitting the SRC2 actions to the *G6pc* promoter together with activities of pterosin B-insensitive unknown factors.

To examine whether pterosin B interrupted the RORα–SRC2 interaction, GAL4-fusion RORα expression constructs were prepared (Fig.3-3A). When full length RORα was used as a bait, detecting the effect of SRC2 overexpression was failed. However, the deletion of the DNA-binding domain from RORα highlighted the coactivator activity of SRC2 (*left panel*), which was promoted by forskolin and suppressed by pterosin B (*right panel*). Because the ROR family is composed of three isoforms, the target isoform for pterosin B was examined. SRC2-dependent RORα activity was suppressed by pterosin B (Fig.3-3B), whereas the activities of RORβ/γ were not clearly affected by SRC2 or pterosin B.

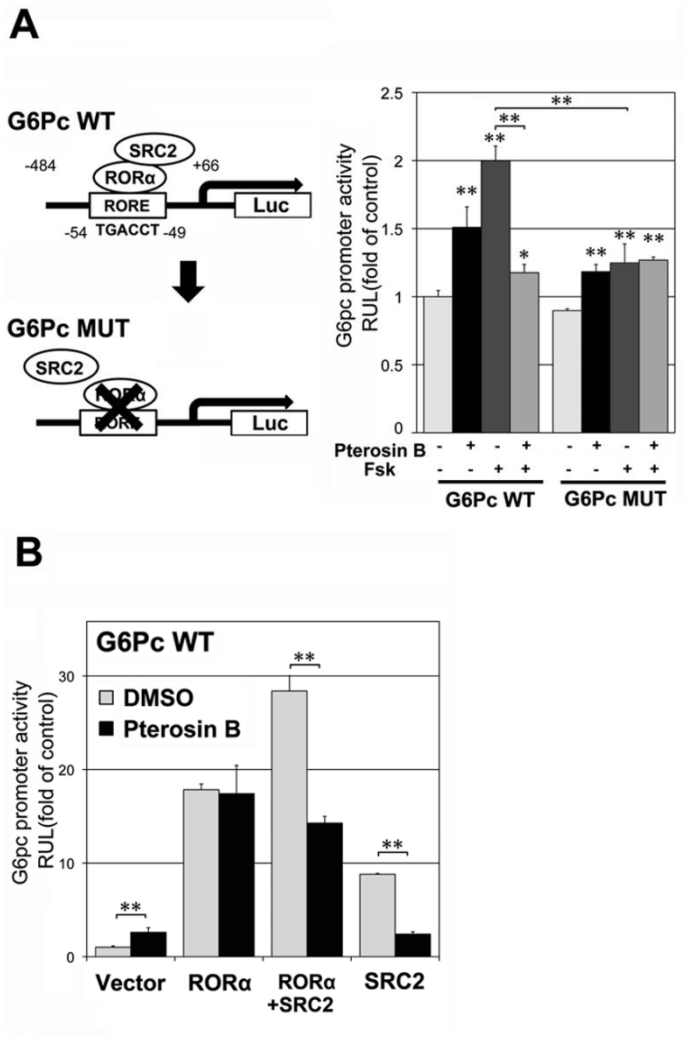

Fig.3-2. Pterosin B disrupts RORα–SRC2.

(A) AML-12 cells transformed with the *G6pc* reporter (WT or mutant, ROR-element disrupted (MUT)) were treated with pterosin B (300 μM) and forskolin (10 μM) for 6 h. *G6pc* promoter–reporter activity (firefly luciferase) was normalized by the internal *Renilla* luciferase activity (TK-rLuc), and the control was set to 1. Means and s.d. are shown (n = 3). *: $p < 0.05$, **: $p < 0.01$. (B) Expression vectors (RORα and SRC2) were co-transformed with the wild-type *G6pc* promoter–reporter vector, and cells were then treated with pterosin B.

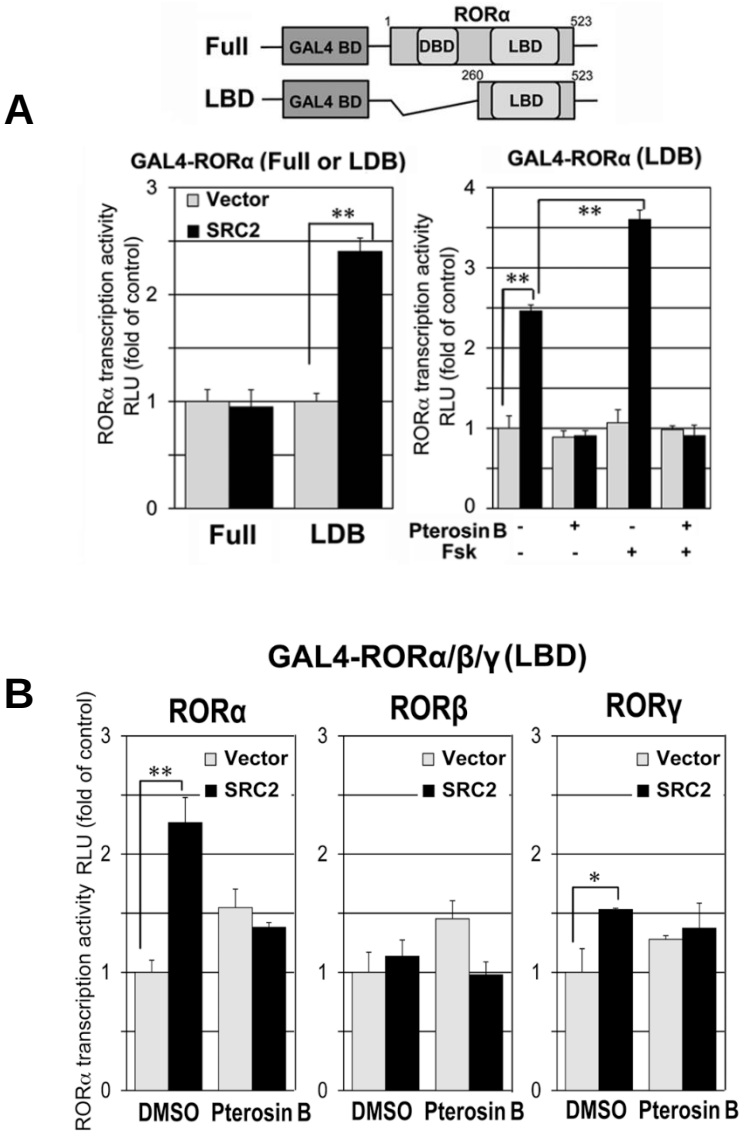

Fig.3-3. Only RORα is affected by SRC2 and pterosin B.

(A) GAL4-fusion RORα (full length and only the ligand-binding domain (LBD)) was expressed as a bait in AML-12 cells. DBD: DNA-binding domain. The RORα transcription activities were evaluated as GAL4 (USA)-Tk-Luc activities, and the effects of SRC2 overexpression on these two RORα activities were examined (*left*). The RORα LBD was used to evaluate the effect of pterosin B or forskolin (*right*). (B) The effects of SRC2 overexpression and pterosin B on the transcription activities of RORα, β, and γ LBD were examined.

Pterosin B interrupts the oxidation-reduction cycle of coenzyme Q

The disruption of *Rorα* in mice (*sg/sg*) resulted in dysregulation of energy metabolism (8). Recently, RORα was found to sense mitochondrial stress in hepatocytes and thereby regulate glycolytic gene expression (9). On the other hand, the *Src2* gene deletion impaired mitochondrial respiration followed by a decrease in ATP production (10). To examine the involvement of pterosin B in mitochondrial energy metabolism, cellular ATP levels in AML-12 cells, maintained under a variety of medium conditions, were measured. When the cells were maintained in glucose-, pyruvate-, and glutamine-free medium, pterosin B lowered the cellular ATP levels (Fig.3-4A). Glucose enhanced cellular ATP levels, and this was not suppressed by pterosin B. However, once the glycolysis inhibitor 2-deoxyglucose was added, glucose-dependent ATP production was reduced by pterosin B, and it completely inhibited pyruvate-induced ATP production, suggesting that pterosin B might suppress ATP production in the mitochondria.

Fig.3-4B illustrates OXPHOS and compounds that have been used in this study. The monitoring of the oxygen consumption rate by the flax analyzer revealed that pterosin B suppressed mitochondrial respiration, which was emphasized as maximum oxygen consumption (Fig.3-4C: the uncoupled state as a result of FCCP treatment).

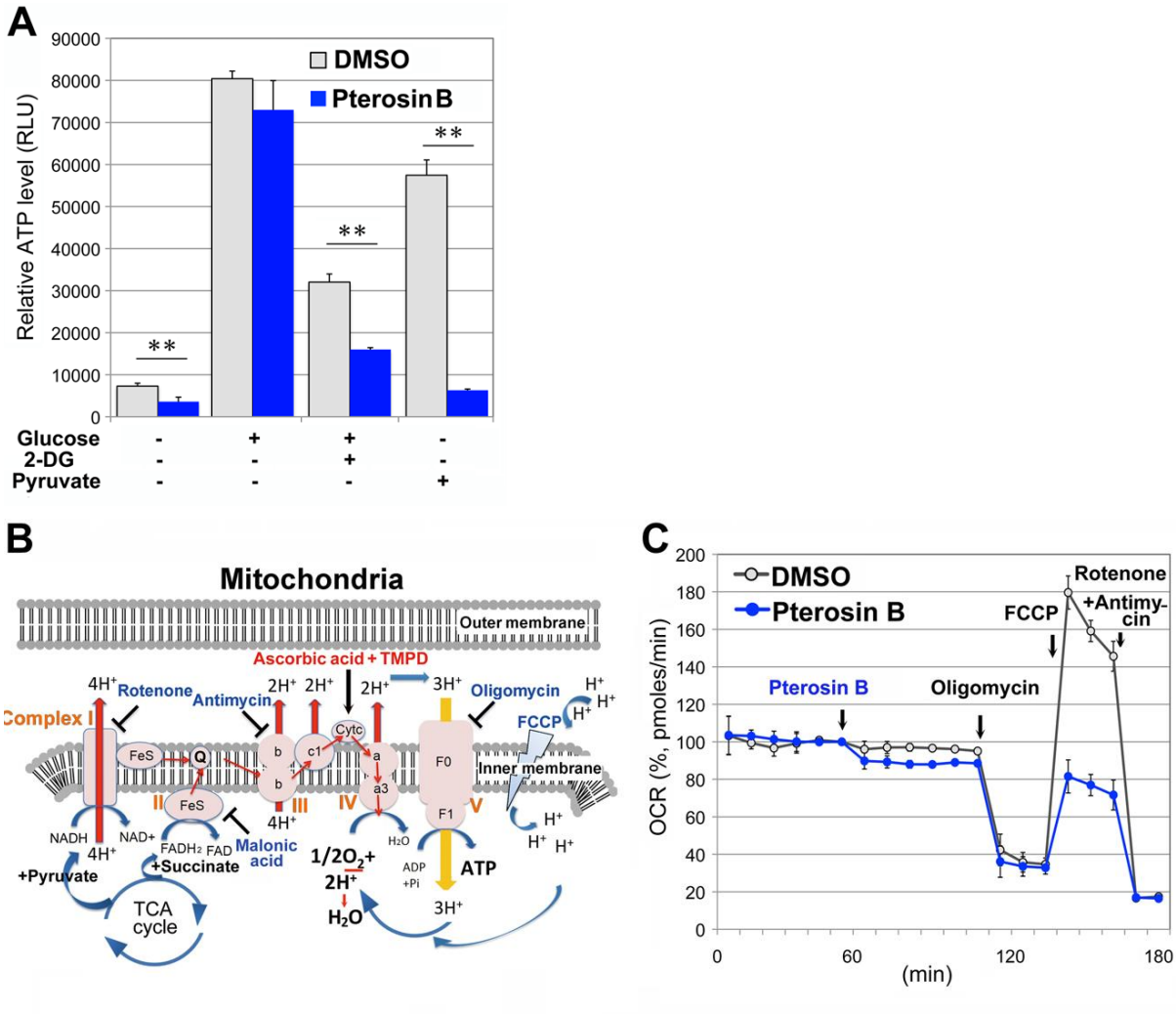

Fig.3-4. Pterosin B impairs oxidation–reduction cycle of coenzyme Q.

(A) AML-12 cells were pre-incubated with DMEM ((-) glucose, pyruvate, and glutamine) for 1 h. Pterosin B (300 μM) was added to the medium, together with 2 mM glucose or 2 mM pyruvate ± 2 mM 2-deoxyglucose (2DG). After 30 min, the cells were lysed to measure ATP levels. Means and s.d. are shown (n = 4). **: $p < 0.01$. (B) Reagents used to analyze mitochondrial oxidative phosphorylation are depicted. Rotenone, malonic acid, antimycin A, and oligomycin are inhibitors for complex I, II, III, and V, respectively. FCCP is an uncoupler that transfers protons from the membrane space to the inner matrix. Ascorbic acid and tetramethyl-*p*-phenylene-diamine (TMPD) reduces cytochrome C (Cytc). Q indicates coenzyme Q. (C) AML-12 cells (n = 3) incubated in DMEM medium supplemented with 2 mM pyruvate and 1 mM glutamine (glucose free) were subjected to oxygen consumption measurements using the flax analyzer. Pterosin B (300 μM) or DMSO was added at indicated time points. Oxygen consumption rate (OCR) for six rounds of measurement was set to 100%. Means and s.d. are shown.

To predict the target of pterosin B in OXPHOS, the levels of ATP and NADH (cellular energy representatives) in the presence of a variety of respiratory toxins were compared (Fig3-5A). As described in Fig3-4A, a high dose of pterosin B decreased cellular ATP levels, which was also observed in the cells treated with other toxins (Fig.3-5B). Pterosin B lowered cellular NAD(P)H levels, whereas, other toxins did not (Fig.3-5C). Interestingly, mitochondrial NADH levels were upregulated by pterosin B or antimycin A (a complex III inhibitor) (Fig.3-5D).

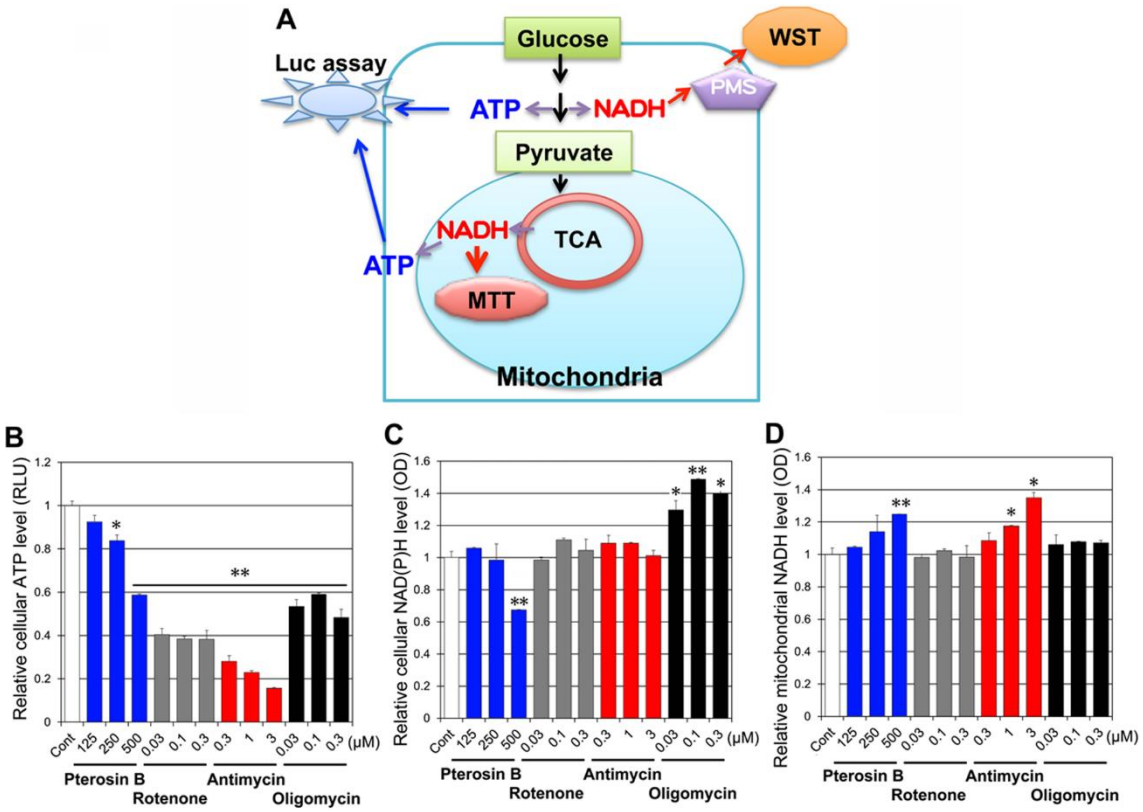

Fig.3-5. Measurement of ATP and NADH

(A) The principle of measurement of ATP and NADH. MTT is reduced by NADH in the mitochondria and converted into colored formazan, whereas water-soluble tetrazolium salt (WST) is reduced in the medium via cytosolic NAD(P)H-dependent reduction of the proton transducer 5-methylphenazinium methylsulfate (PMS). (B) AML-12 cells (n = 4) that had been pre-incubated with DMEM supplemented with 2.5 mM glucose, 1 mM pyruvate, and 1 mM glutamine were treated with indicated doses of pterosin B and respiratory toxins (rotenone, antimycin A, and oligomycin) for 30 min. Cellular ATP (B) and NAD(P)H (C) were measured by using the luciferase (Luc)-based ATP assay kit and WST-8, respectively. Mitochondrial NADH (D) was measured using the MMT assay kit. Means and s.d. are shown. *: $p < 0.05$, **: $p < 0.01$.

Next, ATP production in mitochondria isolated from AML-12 cells was measured (Fig. 3-6). It was defined that oligomycin-inhibited ATP production is the result of OXPHOS. When ATP was produced from carried-over substrate ((-) in Fig.3-6A), pterosin B significantly inhibited ATP production, which was slightly enhanced by the addition of pyruvate plus malate (complex I substrate). While, the pterosin B-dependent suppression of ATP production was weakened by the addition of succinate (complex II substrate). When rotenone (complex I inhibitor) was added to evaluate complex II-dependent electron transfer, pterosin B again inhibited the succinate-dependent ATP production only by 50% (Fig.3-6B), suggesting that complex I pathways might be the main target of pterosin B. On the other hand, once cytochrome c (downstream of complex III) was chemically reduced by adding ascorbic acid plus TMPD in the absence of complex I and II activities, the ATP production was not affected by pterosin B (Fig.3-6C), suggesting that the pterosin B target might be located upstream of complex III and downstream of complex I and II.

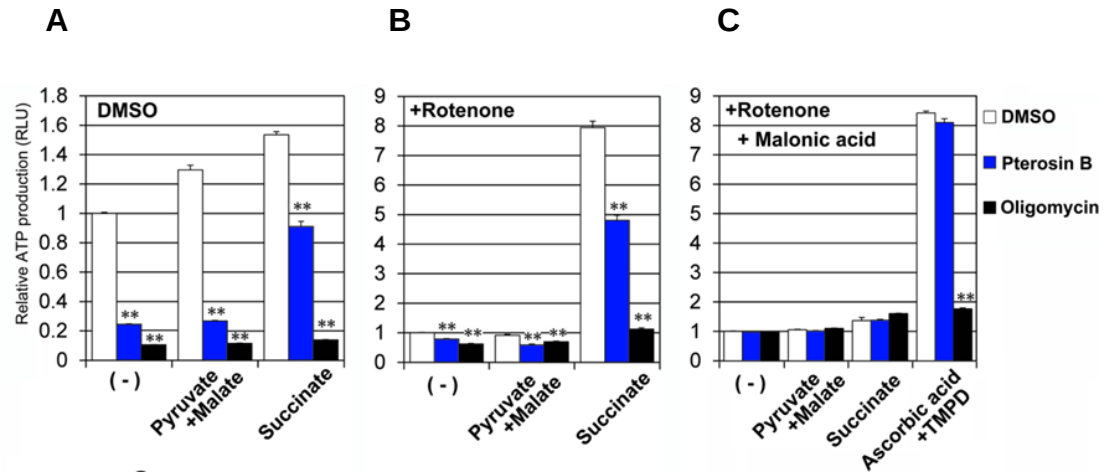

Fig.3-6. Pterosin B inhibits ATP production in mitochondria.

(A) ATP production in isolated mitochondria was initiated by addition of ADP. (-) indicates ATP production from endogenous (carried over) substrates in isolated mitochondria. 100 μM pyruvate plus 100 μM malate were added as complex I substrates. 100 μM succinate was added as the complex II substrate. (B) To evaluate complex II-dependent ATP production, 50 μM rotenone was added. (C) For downstream activation of complex III, complex I and II were inhibited by rotenone and 1 mM malonic acid, and cytochrome C was reduced by 500 μM ascorbic acid plus 125 μM TMPD.

If the complex III (coenzyme Q : cytochrome c–oxidoreductase) was inhibited, the reduced form of coenzyme Q would be allowed to accumulate. To test whether pterosin B affected the oxidation–reduction cycle of coenzyme Q, coenzyme Q was extracted from HEK293 cells that had been treated with pterosin B or antimycin A (Fig.3-7). It was found that pterosin B as well as antimycin A caused the accumulation of reduced coenzyme Q.

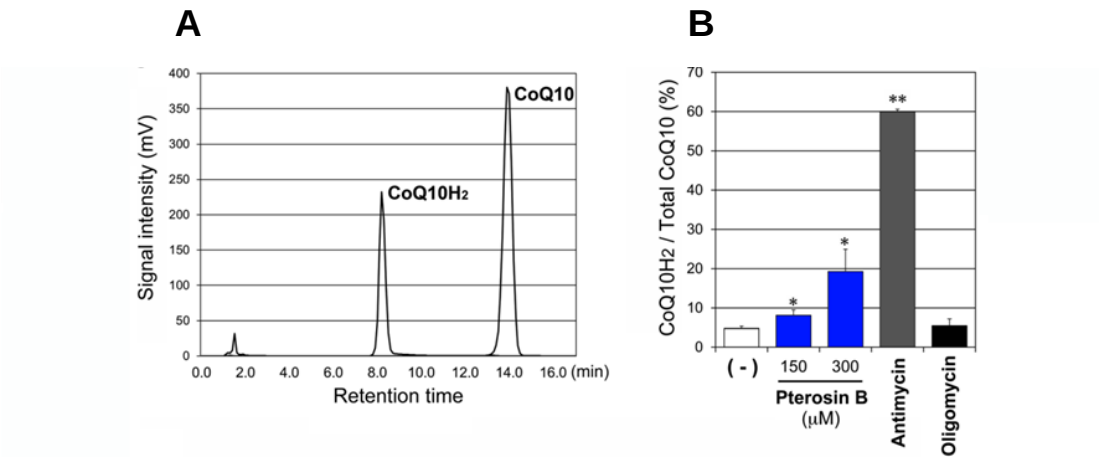

Fig.3-7. Pterosin B impairs oxidation–reduction cycle of coenzyme Q.
(A) Authentic coenzyme Q10 (oxidized: CoQ10 and reduced: $CoQ10H_2$) were separated by HPLC (*left panel*). (B) The percentage of reduced coenzyme Q10 in HEK293 cells that had been treated with pterosin B, antimycin A (3 μM), or oligomycin (0.3 μM) for 30 min is indicated (right panel).

Both pterosin B and antimycin A disrupt RORα–SRC2 signaling

To review the actions of respiratory toxins on gluconeogenic programs, mRNA levels for gluconeogenic gene in AML-12 cells were measured. Forskolin-induced expressions of both *Pparcg1* and *Pck1* were inhibited by rotenone and oligomycin, but not by antimycin A (Fig.3-8A). However, *G6pc* gene expression was inhibited by all the toxins, suggesting the association of multiple regulatory pathways with the *G6pc* promoter. To focus only on RORα–SRC2 actions, GAL4-fusion RORα was used again. Only pterosin B and antimycin A suppressed the SRC2-mediated activation of RORα (Fig.3-8B). Immunoprecipitation followed by western blotting revealed that RORα–SRC2 interactions were disrupted by both pterosin B and antimycin A. On the other hand, all

the toxins activated AMPK, and antimycin A failed to dephosphorylate CRTC2 (Fig.3-8C).

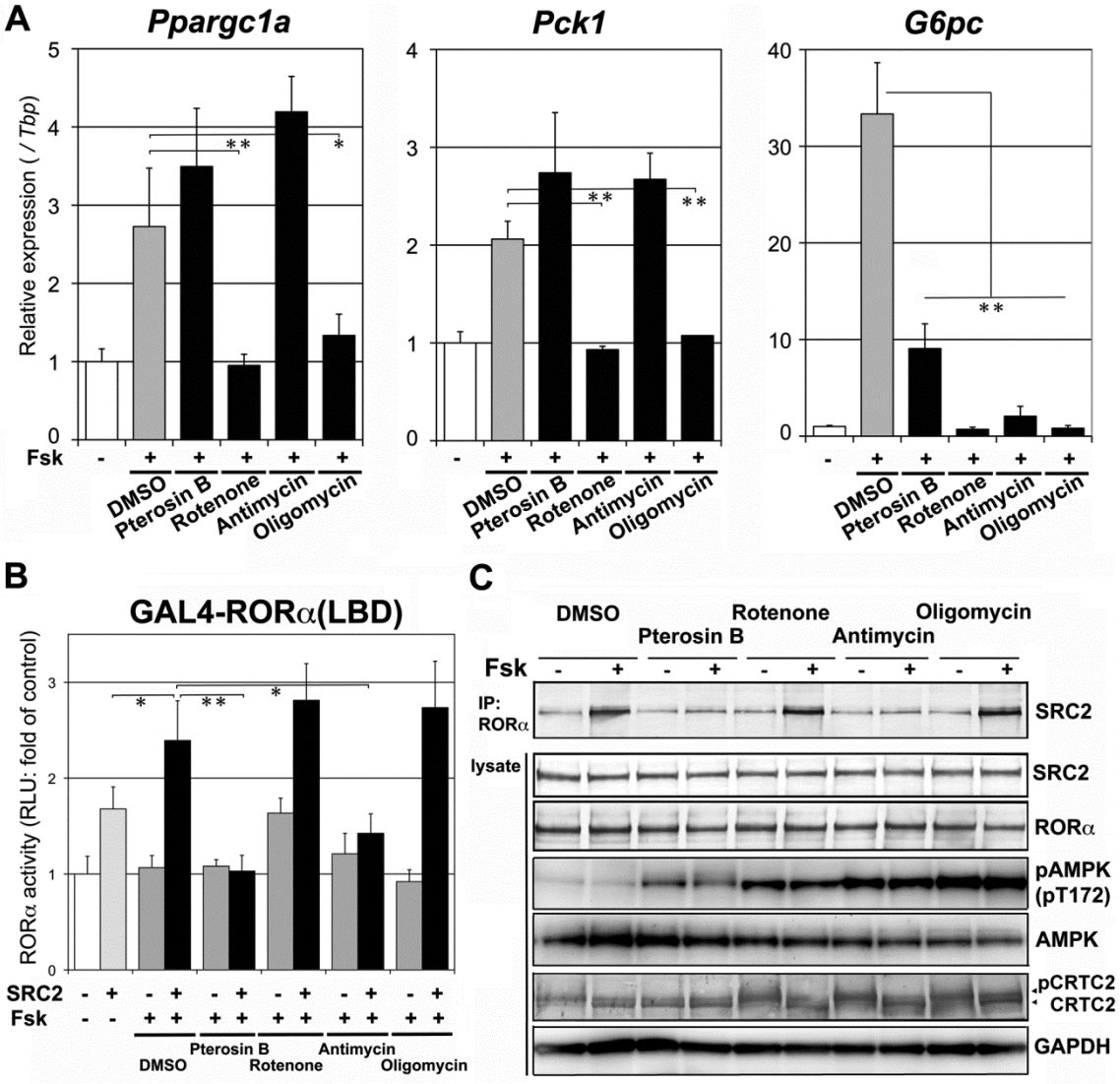

Fig.3-8. Pterosin B and antimycin A specifically disrupt RORα–SRC2.

(A) The mRNA expression of gluconeogenic genes in AML-12 cells that had been treated with forskolin (Fsk, 10 μM) in the presence of various respiratory toxins, rotenone (0.3 μM), antimycin A (3 μM), and oligomycin (0.3 μM) for 2 h was measured using quantitative PCR (n = 3). Means and s.d. are shown. *: $p < 0.05$, **: $p < 0.01$. (B) SRC2-dependent activation of RORα was evaluated by reporter assay using the RORα LBD. Fsk (10 μM) was used to enhance RORα–SRC2-mediated transcription activity. (C) RORα–SRC2 interaction was evaluated by immunoprecipitation.

3-3. Discussion

In this chapter, it has been identified that pterosin B strongly repressed G6pc expression induced by RORa-SRC2 in the cAMP signaling.

Oligomycin (the complex V inhibitor) is often used as a positive control to activate AMPK, followed by a suppression of gluconeogenesis (11,12). In our control experiments, apparently both rotenone (the complex I inhibitor) and oligomycin activated AMPK and suppressed gluconeogenic programs associated with Ppargc1a, Pck1, and G6pc gene expressions. However, pterosin B and antimycin A (the complex III inhibitor) activated AMPK but upregulated Ppargc1a and Pck1 gene expressions.

Both pterosin B and antimycin A interrupted the formation of the RORa-SRC2 complex induced by cAMP, suggesting multiple targets of pterosin B in gluconeogenic programs including coenzyme Q and the RORa-SRC2 complex.

Using pterosin B and antimycin A, an association between OXPHOS and the regulation of RORa was identified. The impairment of complex III activities or the accompanying phenomenon of reduced coenzyme Q accumulation specifically suppressed G6pc expression by disrupting the RORaeSRC2 complex formed by cAMP. Recently, metformin has also been found to lower Src2 expression levels followed by a reduction in G6pc expression (13). Although rotenone (a complex I inhibitor) also suppressed G6pc expression in our study, it did not alter the SRC2 levels or RORaeSRC2 interaction, suggesting that RORa senses a variety of dysregulation in energy homeostasis by different mechanisms, and SRC2 contributes to a part of RORa pathways in gluconeogenic regulation.

Hsu et al. (1) have reported that prolonged treatment with pterosin A causes

hypoglycemic effects in mice and glycogen accumulation in H4IIE hepatoma cells. The activation of AKT by pterosin A is the proposed mechanism by which glycogen synthesis is stimulated through GSK-3b inactivation. On the other hand, G6Pc deficiency in humans also causes excess glycogen storage, which is characterized by hypoglycemia and glycogen accumulation in the liver (7). Similar phenotypes are observed in SRC2- or ROR-deficient mice (5). These evidences suggest that pterosin A- and B-mediated hypoglycemic effects in mice may be the result of a lowered G6pc expression in hepatocytes.

In conclusion, the present results demonstrate that pterosin B has multiple targets in the regulation of hepatic gluconeogensis, including coenzyme Q in RORa-SRC2 signaling.

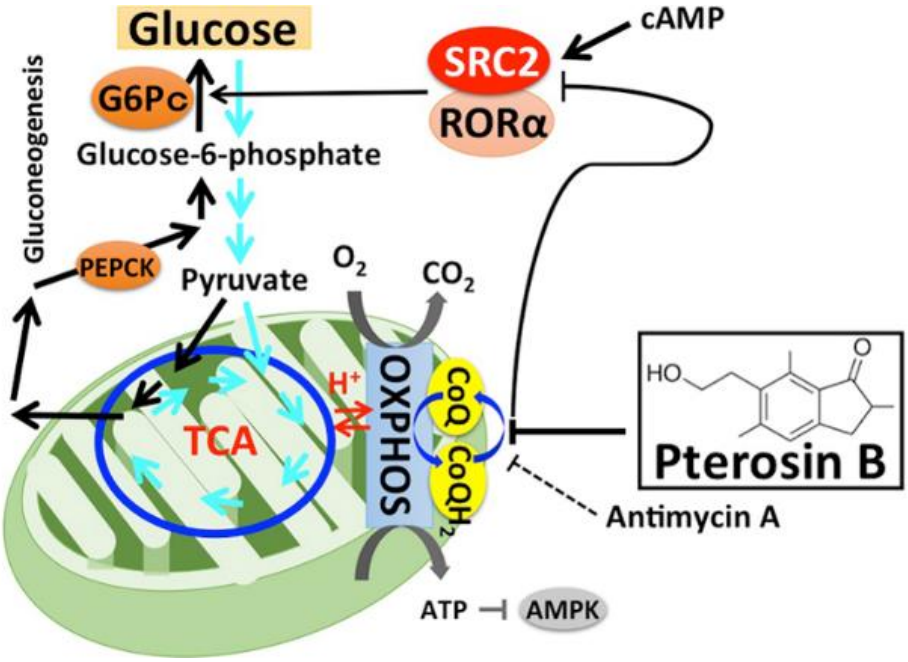

Fig.3-9. Mechanism by which pterosin B regulates hepatic gluconeogenesis in a SIK3-independent manner.

3-4. Reference

1. F.L. Hsu, C.F. Huang, Y.W. Chen, et al., Antidiabetic effects of pterosin A, a small-molecular-weight natural product, on diabetic mouse models, Diabetes 62 (2013) 628-638.
2. D.J. Kojetin, T.P. Burris, REV-ERB and ROR nuclear receptors as drug targets, Nat Rev Drug Discov 13 (2014) 197-216.
3. A.M. Jetten, Retinoid-related orphan receptors (RORs): critical roles in development, immunity, circadian rhythm, and cellular metabolism, Nucl Recept Signal 7 (2009) e003.
4. M. Ermisch, B. Firla, D. Steinhilber, Protein kinase A activates and phosphorylates RORalpha4 in vitro and takes part in RORalpha activation by CaMK-IV, Biochem Biophys Res Commun 408 (2011) 442-446.
5. A.R. Chopra, J.F. Louet, P. Saha, et al., Absence of the SRC-2 coactivator results in a glycogenopathy resembling Von Gierke's disease, Science 322 (2008) 1395-1399.
6. N. Kumar, D.J. Kojetin, L.A. Solt, et al., Identification of SR3335 (ML-176): a synthetic RORalpha selective inverse agonist, ACS Chem Biol 6 (2011) 218-222.
7. R. Froissart, M. Piraud, A.M. Boudjemline, et al., Glucose-6-phosphatase deficiency, Orphanet J Rare Dis 6 (2011) 27.
8. P. Lau, R.L. Fitzsimmons, S. Raichur, et al., The orphan nuclear receptor, RORalpha, regulates gene expression that controls lipid metabolism: staggerer (SG/SG) mice are resistant to diet-induced obesity, J Biol Chem 283 (2008) 18411-18421.
9. J.K. Byun, Y.K. Choi, Y.N. Kang, et al., Retinoic acid-related orphan receptor alpha

reprograms glucose metabolism in glutamine-deficient hepatoma cells, Hepatology 61 (2015) 953-964.

10. S. Dasgupta, N. Putluri, W. Long, et al., Coactivator SRC-2-dependent metabolic reprogramming mediates prostate cancer survival and metastasis, J Clin Invest 125 (2015) 1174-1188.
11. M.R. Owen, A.P. Halestrap, The mechanisms by which mild respiratory chain inhibitors inhibit hepatic gluconeogenesis, Biochim Biophys Acta 1142 (1993) 11-22.
12. W. Hao, C.P. Chang, C.C. Tsao, et al., Oligomycin-induced bioenergetic adaptation in cancer cells with heterogeneous bioenergetic organization, J Biol Chem 285 (2010) 12647-12654.
13. A. Madsen, O. Bozickovic, J.I. Bjune, et al., Metformin inhibits hepatocellular glucose, lipid and cholesterol biosynthetic pathways by transcriptionally suppressing steroid receptor coactivator 2 (SRC-2), Sci Rep 5 (2015) 16430.

Summary

Hepatic gluconeogenic programs are regulated by a variety of signaling cascades. Glucagon-cAMP signaling is the main initiator of the gluconeogenic programs, including G6pc gene expression. In this work, it has been demonstrated that SIK3 has important roles on hepatic gluconeogenesis. To examine the cell autonomous actions of SIK3, screenning of small compounds suppressing SIK3 signaling cascades was conducted. As the result, pterosin B was identified as SIK3 signaling inhibitor. Pterosin B inactivated SIK3 via the activation of PHKG2, resulting in up-regulation of G6pc expression even in the absence of cAMP. In this work, however, it was noticed that once cAMP signaling was initiated, pterosin B became a strong repressor of G6pc expression. The search for associated transcription factors for pterosin B actions revealed that RORa-SRC2 complex on the G6pc promoter was the target. Meanwhile, pterosin B impaired the oxidation-reduction cycle of coenzyme Q in mitochondrial OXPHOS; and antimycin A, an inhibitor of coenzyme Q: cytochrome c-oxidoreductase (termed mitochondrial complex III), also mimicked pterosin B actions on RORa-SRC2 signaling. Although other respiratory toxins (rotenone and oligomycin) also suppressed G6pc expression accompanied by lowered ATP levels following the activation of AMPK, minimal or no effect of these other toxins on RORa-SRC2 activity was observed. These results suggested that individual components in OXPHOS differentially linked to different transcriptional machineries for hepatic gluconeogenic programs, and the RORa-SRC2 complex acted as a sensor for oxidation-reduction cycle of coenzyme Q and regulated G6Pc expression. This was a site disrupted by pterosin B in gluconeogenic programs.

In this work, it has been identified that not only SIK3 but also RORa-SRC2 as a sensor for oxidation-reduction cycle of coenzyme Q could be new targets of diabetes treatment. Screening further compounds regulating these targets is needed.

Experimental Section

$Sik3^{-/-}$ Mice

Embryonic stem cells derived from a C57BL/6N strain (RENKA) were used with the $Sik3^{-/-}$ mice. After mating the mice with C57BL/6J mice (CLEA Japan, Tokyo, Japan) for 3 generations, mouse colonies were expanded for experiments under chow and high-fat-diet feeding. After 7 generations of cross breeding, mice colonies were used for cholesterol and cholic acid experiments. Sik3+/2 mice are now supplied by JCRB Laboratory Animal Resource Bank at the National Institute of Biomedical Innovation (No. nbio157). Information about SIK1-KO, SIK2-KO are described in (13,15), respectively. SIK1-KO mice were mated with C57BL/6J for six generations. The experimental mouse protocols were approved by the ethics committee of the National Institute of Biomedical Innovation (assigned No.DS20-56, 20-77, DS23-37, DS25-54). The animals were maintained under standard conditions of light (0800–2000) and temperature (23uC, 50% humidity). For tissue isolation, all mice were fasted for 4 h and then sacrificed within 61 h of lights out. The chow diet, MF, was purchased from Oriental Yeast (Tokyo, Japan). The high-sucrose (20% cal), high-fat (60% cal), and high-fat (45% cal)/high-sucrose (20% cal) diets were obtained from Research DIET Inc. (NJ,USA). The pre-fasting periods for the glucose tolerance test (GTT), insulin tolerance test (ITT), and lactate tolerance test (LTT) were 4, 2, and 24 h, respectively. We administered 1.5 g/kg glucose, 36 mg/kg insulin, and 1.5 g/kg lactate intraperitoneally for these tests, respectively.

Reagents

Forskolin (Fsk), dexamethasone, glucose oxidase, 4-Aminoantipyrine, *N*-Ethyl-*N*-(2-hydroxy-3-sulfopropyl)-3-methylaniline, sodium salt (TOOS), horseradish peroxidase, oligomycin, 1-propanol, $NaBH_4$ and mannitol were purchased from WAKO Pure Chemicals (Osaka, Japan). Sodium pyruvate solution, oxidized coenzyme Q_{10}, rotenone, carbonilcyanide *p*-triflouromethoxyphenylhydrazone (FCCP), antimycin A, 2-deoxyglucose (2-DG), and *D*-glucose were obtained from Sigma-Aldrich (St. Louis, USA). Sodium malonate solution and trifluoroacetic acid (TFA) were obtained from NACALAI TESQUE, Inc (Kyoto, Japan). HG9-91-01 was obtained from MedChem Express (Monmouth Junction, NJ, USA). Halo-tag expression plasmids for phosphorylase kinase gamma 2 (PHKG2) and other kinases and phosphatases were purchased from Promega (Madison, WI, USA). The anti-AMPK, anti-phospho-AMPK, and anti-phospho-CREB antibodies were from Cell Signaling (Boston, MA, USA), the anti-CREB antibody was from GenScript Corp. (Piscataway, NJ, USA), the anti-GAPDH antibody was from WAKO (Tokyo, Japan), and anti-PHKG2 antibody was obtained from Santa Cruz Biotechnology, Inc. (Dallas, TX, USA). SRC2 and RORα were obtained from Bethyl Laboratories Inc. (Montgomery, TX), Santa Cruz Biosciences Inc. (Dallas, Texas), respectively. Anti-pSIK3 (pT163) was created against the KLH-conjugated peptide (CSNLFTPGQLLK(pT)W, pT: phospho-Thr) in rabbits and purified with the same peptide. CRTC2 protein was separated on an 8% linear polyacrylamide gel, and other proteins were on 4 - 20% gradient gels. AML-12 (alpha mouse liver-12) cells from American Type Culture Collection were cultured in Dulbecco's Modified Eagle Medium (DMEM)-Ham’s F-12 medium supplemented with 10% fetal bovine serum (FBS) and an insulin, transferrin,

and selenium supplement (ITS, Thermo Fisher, Carlsbad, CA, USA).

Information about the knockout (KO) mice, SIK1-KO, SIK2-KO, and SIK3-KO are described in (13,15,18), respectively. SIK1-KO mice were mated with C57BL/6J for six generations. The experimental mouse protocols were approved by the ethics committee of the National Institute of Biomedical Innovation (assigned No.DS20-77, DS23-37, DS25-54). The animals were maintained under standard conditions of light (on: 08:00 – off: 20:00) and temperature (23 °C, 60% humidity). The kinase inhibitor (~90 compounds) libraries were from Enzo Life Science (Farmingdale, NY), and the unannotated compounds (~2000) in the Molport libraries were purchased from Namiki Shouji (Tokyo, Japan). Flavonoids (~50) and other natural compounds (~150) were described in (24,25). Pterosin B was extracted from *Pteridium aquilinum* (total 100 kg, wet) after soaking in 0.1% sodium bicarbonate at 70 °C overnight. The ingredients in the *P. aquilinum* chloroform/hexane (1:4) extract were separated by silica gel and charcoal column chromatography, and pterosin B was crystallized in chloroform by increasing the hexane content. Finally, we got 3 g of pterosin B whose purity was confirmed by nuclear magnetic resonance. Synthetic pterosin B (racemic) was obtained from Intelium Crop. (Tokyo, Japan).

Primary hepatocytes-

Hepatocytes were isolated from mice as described previously (23). Briefly, under isoflurane anesthesia, the mouse livers were perfused with Hanks' balanced salt solution (HBSS) which contained 0.5 mM EGTA, followed by perfusion with Liver Digest Medium (Thermo Fisher). Isolated hepatocytes were cultured in DMEM supplemented with 10% FBS, 100 nM insulin, and 1 μM dexamethasone (1×hepatocyte medium).

Before the treatments, the hepatocytes were incubated with DMEM supplemented with 1% FBS, 10 nM insulin, and 0.1 μM dexamethasone (0.1×hepatocyte medium) for 12 h.

DNA constructs and site-directed mutagenesis-

A cDNA fragment for mouse MEF2C was amplified by means of PCR using primers 5’-TTTTGGATCC(BamHI)ATGGGGAGAAAAAAGATTCAGAT and 5’-TTTTTGCGGCCGC(NotI)TCATGTTGCCCATCCTTCAGAGA, digested with BamHI/NotI and ligated into the pM2 vector. The mammalian expression vector, pCMVsport6, containing full-length mCRTC2 (IMAGE: 5345301) cDNA, was purchased from Invitrogen. cDNA was digested with BamHI-NotI, and the TORC2 cDNA fragments was ligated into the BamHI–NotI site of a GFP expression vector pEGFP-C for cytochemical studies and a pM vector (Gal4-fusion) for reporter assays. The SIK3 mutants (S493A, T411A, and the double Ala mutant (DA)) were constructed by site-directed mutagenesis using pTarget-hSIK3 plasmids and the following primers: for S493A (5'-CCCTTGGCCGGAGGGCTGCAGATGGAGGAGCCAAC/5’-GTTGGC TCCTCCATCTGCAGCCCTCCGGCCAAGGG), and for T411A 5’-TTGTCAATGAGGAGGCATGCCGTGGGTGTGGCTGACCCA/5’-TGGGTCAG CCACACCCACGGCATGCCTCCTCATTGACAA). The SIK3 DA mutant was constructed by using pTarget-hSIK3 S493A as the template with the primers for T411A. To prepare an adenovirus vector for SIK3 (WT, DA), the SIK3 cDNA fragments were amplified by PCR with the attB primers. The amplified products were then constructed into pDONR221 vectors by using BP clonase enzyme mix (Thermo Fisher). The resultant cDNAs were finally cloned into pAd/DMV/V5-DEST Gateway vectors using

LR clonase enzyme mix (Thermo Fisher). To screen the SIK3 inhibitory compounds, we constructed the LexA reporter assay system. A DNA fragment containing 3×LexA elements was prepared by annealing the oligonucleotides 5'-GATCTACTGTATATATATACAGTAGAGTACTGTATATATATACAGTACAC TACTGTATATATATACAGTA/5'-AATTTACTGTATATATATACAGTAGTGTAC TGTATATATATACAGTACTCTACTGTATATATATACAGTA) and the fragment was ligated into the *Bgl* II / *Eco*R I site of the *Renilla*-Luc internal reporter vector (pRL-TK). To prepare the LEXA-CRTC2 expression vector, a DNA fragment for LEXA DNA-binding domain was amplified by PCR with primers (5'-GCAAAAAGCTAGATCATGAAAGCGTTAACGGCCAGGCAA/5'-ACCATAA TGAGAGTCCAGCCAGTCGCCGTTGCGAA) and *E. coli* genome DNA. An In-Fusion HD Cloning Kit (Clontech, Mountain View, USA) was used to replace the DNA fragment for the GAL4 DNA-binding domain in the pM-CRTC2 vector with the LEXA fragments in pM-CRTC2. The HEK293 cells were placed into 96-well white-bottom plates and transfected with the SIK3 expression vectors (WT or its empty vector; 5 ng), DNA-binding domain-linked expression vectors (pM-MEF2C and pMLexA-CRTC2; 5 ng), pTAL-GAL4 (20 ng), and pRL-LexA (20 ng) per well, using Lipofectamine 2000 (Thermo Fisher). To measure the reporter activity, we used the Dual-Luciferase Reporter Assay System (Promega). The cells were lysed with 10 μL of passive lysis buffer, and all of the lysate was used for the assay.

Quantitative real-time PCR analysis

The total RNA was extracted using an EZ1 RNA Universal Tissue Kit (Qiagen, Venlo, Netherlands), and the cDNA was synthesized using a ReverTra Ace qPCR RT Master Mix (TOYOBO, Kyoto, Japan). PCR amplification was performed using an EXPRESS SYBR GreenER (Thermo Fisher). Primers used in this study were *Pgc1a* (5'-GCGAACCTTAAGTGTGGAAC/5'-CACCACGGTCTTGCAAGAGG), *Pepck* (5'-AGAACAAGGAGTGGAGACCG/5'-GCTTCATAGACAAGGGGGAC), *G6pc* (5'-CGCAGCAGGTGTATACTATG/5'-CCCAGAATCCCAACCACAAG), and *Tbp* (5'-GAGCTCTGGAATTGTACCGC/5'-TGTGCACACCATTTTTCCAG). Levels of gluconenogenic mRNA were normalized by *Tbp* mRNA.

Reporter assay

HEK293 and AML-12 cells were transfected with the SIK3 expression vectors (pTarget hSIK3 WT, T411A, S493A, T411A/S493A [DA] or its empty vector; 50ng), GAL4 DNA-binding domain-linked expression vectors (pM-MEF2C, pM-CRTC2 or its empty vector; 50ng), pTAL-GAL4 (150ng), and the *Renilla*-Luc internal reporter (pRL-(Int-)TK, 50ng) using Lipofectamine 2000 reagent (Thermo Fisher). To measure reporter activity, we used the Dual-Luciferase Reporter Assay System (Promega). The cells were lysed with 100 μL of passive lysis buffer, and 10 μL was used for the assay. The activities of firefly luciferase were normalized by those of *Renilla* luciferase. The reporter activity measurement was performed as described above. The cells were lysed with 100 μL of passive lysis buffer, and 10 μL was used for the assay. The activities of firefly luciferase were normalized by those of *Renilla* luciferase. To construct vectors for miRNA(s) against PHKG2, double-stranded oligonucleotides (No. 1: 5′-

TGCTGAGAATGTGCATCTCTCGCCGTGTTTTGGCCACTGACTGACACGGCGA GATGCACATTCT/5′-CCTGAGAATGTGCATCTCGCCGTGTCAGTCAGTGGCCA AAACACGGCGAGAGATGCACATTCTC and No. 2: 5′-TGCTGTCCAGTAGAGACCTCATGATGGTTTTGGCCACTGACTGACCATCA TGATCTCTACTGGA/5′-CCTGTCCAGTAGAGATCATGATGGTCAGTCAGTGGC CAAAACCATCATGAGGTCTCTACTGGAC) were introduced into the pcDNA6.2-GW/EmGFP-miR vector (Life Technologies), and adenoviruses were prepared by the Gateway system. Knockdown of PHKG2 protein in AML-12 cells was achieved by 2 times infection / transformation with 2 days interval.

The *G6pc* luciferase gene including the promoter sequence was amplified with mouse genomic DNA and the primers (*G6pc prom F/R* in Supplementary Materials). PCR products were cloned into the pGL3 vector. The *G6pc* mutant was constructed by site-directed mutagenesis using pGL3 *G6pc* plasmids and the primers (*G6pc prom MutF and MutR)*. Halo-tagged RORα and SRC2 expression plasmids were purchased from Promega (Madison, WI). The plasmids were reconstructed into the pcDNA3.2 vector. GAL4-RORα/β/γ cDNA fragments were amplified with the following primers: RORα F/R, RORβ F/R, and RORγ F/R in Supplementary Materials and then ligated into the pM vector (the *Bam* HI- *Not* I site that was created in a previous study). The AML-12 cells were plated onto 24-well-plates and transfected with pGL3-*G6pc* WT, mutant, or empty vector (200 ng): *Runilla*-Luc internal reporter [pRL-(Int) TK, 50ng], pcDNA3.2-RORα (50 ng), and pcDNA3.2-SRC2 (50 ng). The reporter activity was measured using Dual-Luciferase Reporter Assay System (Promega).

Glucose production and cAMP measurement

Primary hepatocytes were seeded on a 24-well plate (1.0×106) and incubated in an 1×hepatocyte medium for 3 h and then in an 0.1×hepatocyte medium for 12 h. The AML-12 cells were plated in 24-well plate (1.0×106) and incubated in DMEM/F-12 medium for 72 h (with medium change every 24 h) to increase the cellular lipid droplets. After the medium replacement with 0.1×hepatocyte medium, the cells were further cultured for 12 h. The glucose production assay was performed as described (22). Briefly, the cells were washed with phosphate buffer saline followed by adding 300 μL of assay medium (DMEM without glucose or glutamate containing 1 mM sodium pyruvate, 10 mM lactate, and 100 nM dexamethasone) containing the compounds (Fsk *etc.*) per well. After approximately 0-8 h of incubation, the assay medium was harvested and centrifuged at 12,000 rpm for 10 min. Then, 20 μL of the supernatant was used for the assay. To measure the glucose levels, 180 μL of reaction buffer (50 mM sodium phosphate (pH 7.0), 1 U/mL glucose oxidase, 0.1 U/mL horse radish peroxidase, 50 μM 10-acetyl-3,7-dihydroxyphenoxazine, ADHP) was added to each well of a 96-well black plate and incubated at room temperature for 30min. The fluorescence at 590 nm was measured with excitation at 535 nm. The AML-12 cells were placed into a 96-well plate at a density of 2.0×104. The pGloSensor-22F cAMP Plasmids (Promega) were transfected into the cells using Lipofectamine 2000. The cAMP levels were detected with chemiluminescence using GloSensor cAMP Reagent (Promega).

Purification of SIK3 and in vitro kinase activity

The pEBG-hSIK3 WT vector was transfected into the HEK293 cells. After 36 h of transfection, the cells were lysed with IP lysis buffer (50 mM Tris-HCl (pH 8.0), 5 mM EDTA, 5 mM EGTA, 2 mM DTT, 50 mM glycerol 3-phosphate, 50 mM NaF, 1 mM NaVO4, 0.5% Triton X-100, 1 mM phenylmethylsulfonyl fluoride, 10 μg/mL leupeptin, and 14 μg/mL aprotinin) and incubated with glutathione sepharose 4B (GE Healthcare, Waukesha, USA) at 4 °C for 15 min. The protein complexes were washed with IP lysis buffer and eluted with 10 mM of glutathione. Aliquots of purified SIK3 were subjected to an *in vitro* kinase assay and Western blot analyses. Adenoviruses of hSIK3 WT and DA was transfected to AML-12 cells. After the stimulation with Pterosin B and Fsk, the cells were lysed with 1 mL of IP lysis buffer and incubated with Protein G Sepharose (GE Healthcare) containing anti-SIK3 antibody at 4 °C for 1 h. Purified SIK3 was eluted with 100 μL of 3×SDS and detected by western blot analyses. The purified SIK3 enzyme was incubated with coumarin-labeled CRTC2 peptides and compounds in 40 μL of reaction buffer (5 mM Tris-HCl (pH 7.4), 1 mM ATP, 1 mM DTT, 5 mM MgCl2). The reactions were performed at 25 °C for 1 h and were stopped by the addition of 40 μL of 3×SDS sample buffer. The phosphorylated peptide was separated by electrophoresis on a 1.5% agarose gel in 50 mM Tris–borate buffer (pH 8.5) and visualized by ultraviolet light (28). The PHKG2 enzyme was also prepared by the same methods as for SIK3 and incubated with coumarin-labeled SIK3 T411 peptide (KKLSMRRHTVGVADP) or S493 peptide (KKPLGRRASDGGANI) in 40 μL of the reaction buffer (5 mM Tris-HCl [pH 6.8], 1 mM ATP, 1 mM DTT, 5 mM MgCl2). The phosphorylated peptide was separated on the agarose gel in 50 mM Tris–acetate buffer (pH 3.5).

Glycogen measurement

AML-12 cells were lysed in 0.1 M sodium citrate buffer (pH = 4.2) supplemented with 60 mM NaF, and the supernatants were recovered by centrifugation at 14,000 *g* for 5 min. The concentration of glycogen was measured using the EnzyChrom Glycogen Assay Kit (BioAssay Systems, Hayward, CA, USA). Reagents for Periodic acid–Schiff (PAS) stain were obtained from Mutokagaku Co. Ltd. (Tokyo, Japan).

Cellular ATP and NADH levels

AML-12 cells were plated onto 96-well plates. The following day, cells were pre-treated for 1 h with DMEM (free of glucose, pyruvate, and glutamine). The medium was changed for 1 h to a reaction medium containing pterosin B (300 μM) ± 2 mM glucose, 2 mM pyruvate, and 2-DG. ATP was measured using an ATP measurement reagent (TOYO B-net, Tokyo, Japan). NADH was measured using the Cell Counting Kit-8 or 3-(4,5-dimethylthiazol-2-yl)-2,5-diphenyltetrazolium bromide (MTT)-assay Kit (Dojin, Tokyo, Japan).

Isolation of mitochondria from AML-12 cells

AML-12 cells were plated into 15-cm dishes at a density of 2×10^6. After 2 days in culture, cells were harvested using 5 ml of extraction buffer (10 mM HEPES, 200 mM mannitol, 70 mM sucrose, and 1 mM EGTA) followed by homogenization in a 10-mL Dounce homogenizer. The homogenized cells were centrifuged at 600 × g for 5 min at 4°C. The supernatant was then was centrifuged at 11,000 × g for 10 min. The supernatant was removed, and pellets were washed with 1 mL of reaction buffer (300 mM mannitol, 10 mM KCl, 5 mM $MgCl_2$, 10 mM potassium phosphate, and 10 mM

Tris-HCl with pH 6.8). After centrifugation at 11,000 × g for 10 min, pellets were re-suspended in 500 µL of reaction buffer containing bovine serum albumin (2 mg/mL).

Mitochondrial ATP production assay

One milligram of mitochondria was mixed with the reaction buffer containing 100 µM ADP, substrates (100 µM pyruvate and 100 µM malate as complex I substrate, 100 µM succinate as complex II substrate, and 500 µM ascorbic acid plus 125 µM TMPD for the reduction of cytochrome C), and inhibitors (500 µM pterosin B, 50 µM rotenone as complex I inhibitor, 1 mM malonic acid as complex II inhibitor, and 100 µM oligomycin as complex V inhibitor). The mixture was incubated at 25°C for 10 min. Five microliters of the mixture was added to 30 µL of ATP measurement reagent (see above) followed by the addition of 25 µL of water.

HPLC analysis of *coenzyme Q_{10} from HEK293 cells*

Mouse cells (such as AML-12) have coenzyme Q_9, and human cells have coenzyme Q_{10}. Because we could obtain only coenzyme Q_{10} standards, human embryonic kidney 293A cells (HEK293A, Thermo Fisher Scientific) were used. These cells were plated onto 10-cm dishes and were incubated for 1 h with pterosin B the following day. Washed cells were harvested in 1 mL of trypsin and centrifuged at 1500 rpm for 10 min. The cell pellets were suspended in PBS, followed by lysis with 1.5 mL of ethyl acetate. The extracts were centrifuged at 1500 rpm for 10 min, and the upper layer was transferred into new tubes. The organic layer was then dried and dissolved in 20 µL of 1-propanol. Ten microliters was used for HPLC analysis [1].

The oxidized form of coenzyme Q_{10} was reduced with $NaBH_4$ to yield coenzyme

$Q_{10}H_2$. Briefly, 200 μL of 100 μM coenzyme Q_{10} was reacted with 5 μL of 100 μM $NaBH_4$ at room temperature in a dark place. Coenzyme $Q_{10}H_2$ extraction was performed as previously described and dissolved in 100 μL of 1-propanol [2]. Reduced and oxidized forms of coenzyme Q_{10} were separated by HPLC. HPLC operating conditions were established as follows: COSMOSIL 5C_{18}-MS-II, 4.6 mm × 100 mm (NACALAI TESQUE, Inc); 20% 1-propanol, 0.05% TFA in methanol as the mobile phase; isocratic mode at a flow rate of 1 mL/min; and UV detection at 275 nm.

Measurement of oxygen consumption

Oxygen consumption was measured using the Seahorse XF24 Flux Analyzer (Seahorse Bioscience, Billerica, USA). AML-12 cells were plated onto 24-well XF24 cell culture plates at a density of 3×10^5. The following day, the culture medium was changed to the assay medium (DMEM) containing 2.5 mM glucose, 1 mM pyruvate, and 0.5 mM glutamine. Mitochondrial function was determined using a sequential injection of pterosin B, oligomycin, FCCP, and rotenone plus antimycin A.

Western blotting and immunoprecipitation (IP)

AML-12 cells that had been plated onto 6-well plates were stimulated with inhibitors and forskolin for 1 h were lysed with 1 mL of IP lysis buffer (50 mM Tris-HCl with pH 8.0, 5 mM EDTA, 5 mM EGTA, 2 mM DTT, 50 mM glycerol 3-phosphate, 50 mM NaF, 1 mM $NaVO_4$, 0.5% Triton X-100, 1 mM phenylmethylsulfonyl fluoride, 10 μg/mL leupeptin, and 14 μg/mL aprotinin) [3] and incubated with Protein G Sepharose (GE Healthcare) containing RORα antibody at 4°C for 1 h. Purified RORα was eluted with 50 μL of 3 × SDS and detected by western blot analysis.

Statistical analyses

Data from each group were characterized by the mean±SD. Student's *t*-test was used to assess all experimental data in Microsoft Excel.

Abbreviation

SIK: Salt-inducible kinase

AMPK: 5′-AMP-activated protein kinase

cAMP: cyclic adenosine monophosphate

CREB: cAMP responsive element binding protein

CRTC: CREB-regulated transcription coactivator

HDAC: histone deacetylase

PKA: cAMP-activated protein kinase

MEF2: myocyte enhancer factor 2

Pepck: phosphoenolpyruvate carboxykinase

G6pc: glucose-6-phosphatase catalytic subunit

Pgc1a: peroxisome proliferator-activated receptor gamma coactivator 1α

AML-12: alpha mouse liver-12

DMEM: Dulbecco's Modified Eagle Medium

ITS: insulin, transferrin, and selenium supplement

Fsk: forskolin

STS: staurosprine

fLuc: firefly luciferase

rLuc: *Renilla* luciferase

GFP: green fluoresce protein

LKB1: liver kinase B1

CaMK: Ca^{2+}/calmodulin-dependent protein kinase

PP1CA: protein phosphatase 1, catalytic subunit, alpha isozyme

PP2CA: protein phosphatase 2, catalytic subunit, alpha isozyme

Cn: protein phosphatase 3, catalytic subunit, alpha isozyme

PDK2: pyruvate dehydrogenase kinase, isozyme 2

PDK4: pyruvate dehydrogenase kinase, isozyme 4

PDP1: pyruvate dehyrogenase phosphatase catalytic subunit 1

PDP2: pyruvate dehyrogenase phosphatase catalytic subunit 2

PHKG1: phosphorylase kinase, gamma 1

PHKG2: phosphorylase kinase, gamma 2

RORa: retinoic acid receptor-related orphan receptor alpha;

SRC2: steroid receptor coactivator 2

OXPHOS: oxidative phosphorylation

FCCP: carbonilcyanide p-triflouromethoxyphenylhydrazone

2-DG: 2-deoxyglucose

TFA: trifluoroacetic acid

ADP: adenosine 5'-diphosphate

qPCR: quantitative real time PCR.

List of Publications

Accepted Journal Papers with review

1. Horike N, Kumagai A, Shimono Y, Onishi T, **Itoh Y**, Sasaki T, Kitagawa K, Hatano O, Takagi H, Susumu T, Teraoka H, Kusano K, Nagaoka Y, Kawahara H, Takemori H. Downregulation of SIK2 expression promotes the melanogenic program in mice. ***Pigment Cell Melanoma Res.*** (2010) 23(6):809-19

2. Kumagai A, Horike N, Satoh Y, Uebi T, Sasaki T, **Itoh Y**, Hirata Y, Uchio-Yamada K, Kitagawa K, Uesato S, Kawahara H, Takemori H, Nagaoka Y. A potent inhibitor of SIK2, 3, 3', 7-trihydroxy-4'-methoxyflavon (4'-O-methylfisetin), promotes melanogenesis in B16F10 melanoma cells. ***PLoS One*** (2011) 6: e26148.

3. Uebi T, **Itoh Y**, Hatano O, Kumagai A, Sanosaka M, Sasaki T, Sasagawa S, Doi J, Tatsumi K, Mitamura K, Morii E, Aozasa K, Kawamura T, Okumura M, Nakae J, Takikawa H, Fukusato T, Koura M, Nish M, Hamsten A, Silveira A, Bertorello AM, Kitagawa K, Nagaoka Y, Kawahara H, Tomonaga T, Naka T, Ikegawa S, Tsumaki N, Matsuda J, Takemori H. Involvement of SIK3 in glucose and lipid homeostasis in mice. ***PLoS One***. (2012) 7:e37803 ○CHAPTER1

4. Kumagai A, Fujita A, Yokoyama T, Nonobe Y, Hasaba Y, Sasaki T, **Itoh Y**, Koura M, Suzuki O, Adachi S, Ryo H, Kohara A, Tripathi LP, Sanosaka M, Fukushima T, Takahashi H, Kitagawa K, Nagaoka Y, Kawahara H, Mizuguchi K, Nomura T, Matsuda J, Tabata T, Takemori H. Altered Actions of Memantine and NMDA-Induced Currents in a New Grid2-Deleted Mouse Line. ***Genes*** (2014) 5: 1095-1114.

5. Sanosaka M, Fujimoto M, Ohkawara T, Nagatake T, **Itoh, Y**, Kagawa M, Kumagai A, Fuchino H, Kunisawa Jun, Naka T, Takemori H. SIK3 deficiency exacerbates LPS-induced endotoxin shock accompanied by increased levels of proinflammatory molecules in mice. ***Immunology*** (2015) 145 (2):268-278

6. **Itoh Y**, Sanosaka M, Fuchino H, Yahara Y, Kumagai A, Takemoto D , Kagawa M, Doi J, Ohta M, Tsumaki N, Kawahara N, Takemori H. SIK3 signaling is important for the gluconeogenic programs in mouse hepatocytes. ***J. Biol. Chem*** (2015) 290(29):17879-93 ○CHAPTER1, CHAPTER2

7. Yamahara M, Sugimura K, Kumagai A, Fuchino H, Kuroi A, Kagawa M, **Itoh Y**, Kawahara, H, Nagaoka Y, Iida O, Kawahara N, Takemori H, Watanabe H. Callicarpa longissima extract, carnosol-rich, potently inhibits melanogenesis in B16F10 melanoma cells. ***J. Nat. Med.*** (2015) 70(1):28-35

8. Kumagai A, Yanagihara K, Suga M, **Itoh Y**, Takemori H, Furue MK. A Simple Method for Labeling Human Embryonic Stem Cells Destined to Lose Undifferentiated Potency. ***Stem Cell Trnas. Med.*** (2016) 5(3):275-81

9. Yahara Y, Takemori H, Okada M, Kosai A, Yamashita A, Kobayashi T, Fujita K, **Itoh Y**, Nakamura M, Fuchino H, Kawahara N, Fukui N, Watanabe A, Kimura T, Tsumaki N. Pterosin B prevents chondrocyte hypertrophy and osteoarthritis in mice by inhibiting Sik3. ***Nat. commun.***(2016) 7:10959

10. **Itoh Y**, Fuchino H, Sanosaka M, Kako K, Hada K, Fukamizu A, Takemori H, Kawahara N. Pterosin B has multiple targets in gluconeogenic programs, including coenzyme Q in RORα–SRC2 signaling. ***Biochem Biophys Res Commun.*** (2016) 473(2):415-20　○CHAPTER3

11. **Itoh Y**, Nagaoka Y, Katakura Y, Kawahara H, Takemori H. Simple chronic model using hypopigmented mice with a *Hermansky-Pudlak syndrome 5* gene mutation. ***Pigment Cell Melanoma Res.*** (2016) 29(5):578-82

Conference Presentations

International academic conferences

1. **Itoh Y**, Uebi T, Kumagai A, Sanosaka M, Takemori H. SIK3 is a new regulator of lipid homeostasis in the mouse liver. Experimental Biology (2012) San-Diego　平成 24 年 4 月 22 日　○CHAPTER1

2. **Itoh Y**, Sanosaka M, Kumagai A, Takemori H, Fuchino H, Kawahara N, Doi J, Ohta M. Effects of Pterosin B from Pteridium Aquilinum on the blood glucose level in db/db mice. The EMBO meeting (2013)
Amsterdam　　平成 25 年 9 月 22 日　○CHAPTER3

National academic conferences

1. 伊東祐美、上尾達也、熊谷彩子、早坂直人、秦野修、竹森洋．塩誘導性キナーゼ SIK は核内受容体の反応性を決定する．日本生化学会大会　(2010) 口頭及びポスター発表　平成 22 年 12 月
2. 伊東祐美、上尾達也、熊谷彩子、竹森洋．塩誘導性キナーゼ SIK3 はコレステロールを補充したバランス食を解毒する．日本生化学会大会　(2011)　ポスター発表　平成 23 年 9 月
3. 伊東祐美、上尾達也、熊谷彩子、竹森洋、土居純子．塩誘導性キナーゼ SIK3 はコレステロールのクリアランスを制御する．日本栄養・食糧学会大会　(2012)　口頭発表　平成 24 年 5 月

4. 伊東祐美、佐野坂真人、熊谷彩子、竹森洋．SIK3 によるクラスⅡ-HDAC 制御がコレステロール-胆汁酸代謝へ与える影響．日本生化学会大会　(2012) ポスター発表　平成 24 年 12 月
5. 伊東祐美、佐野坂真人、熊谷彩子、竹森洋、渕野裕之、土居純子、太田美穂．ワラビ Pterosin の db/db マウスにおける血糖値低下作用．日本栄養・食糧学会大会　(2013)　口頭発表　　平成 25 年 5 月　○CHAPTER3
6. 伊東祐美、佐野坂真人、熊谷彩子、竹森洋、渕野裕之、土居純子、太田美穂．ワラビ Pterosin の ATP 産生抑制作用．日本栄養・食糧学会大会　(2014)　口頭発表　平成 26 年 6 月　○CHAPTER3
7. 伊東祐美、佐野坂真人、熊谷彩子、渕野裕之、川原信夫、竹森洋．肝糖新生における LKB1 下流因子 AMPK と SIK3 の重要性について．日本生化学会大会　(2014)　口頭及びポスター発表　平成 26 年 12 月　○CHAPTER2
8. 伊東祐美、渕野裕之、川原信夫、竹森洋．ワラビ Pterosin B の Forskolin 誘導性 G6Pc 遺伝子の抑制機構．日本生化学会（2015）ポスター発表　平成 27 年 12 月　○CHAPTER3

Acknowledgement

I am deeply grateful to Professor Hidehisa Kawahara for his helpful guidance in my ph.D work and preparing for this dissertation.

I would like to thank Professor Yasuo Nagaoka and Professor Munehiro Yoshida for their helpful guidance in my ph.D work.

I would like to express my gratitude to Dr. Hiroshi Takemori for giving an opportunity of this research and helpful guidance.

I would like to thank Dr. Tatsuya Uebi, Dr. Ayako Kumagai and Dr. Masato Sanosaka for their helpful advice and kind support.

I would like to show my greatest appreciation to Dr. Nobuo Kawahara, Dr. Hiroyuki Fuchino, Professor Miho Ohta and Professor Junko Doi for their helpful advice in my research.

I also would like to thank Mrs. Junko Morita, Ms. Tomoko Onishi, Ms. Mai Kagawa and Ms. Maiko Ohkubo for their technical supports.